Sustainable Cities and Society 130 (2025) 106576

Contents lists available at ScienceDirect

Sustainable Cities and Society

journal homepage: www.elsevier.com/locate/scs

Exploring the characteristics of "Demolition for Green" and its impact on urban thermal environments: An empirical study of Beijing, China

Linchun Zhang [a,1], Zhi Cai [b,*], Huanchun Huang [c,**,1], Zefeng Lu [a], Wei Zhai [c], Haoming Qin [c], Zhifeng Liu [d], Yan Tang [e]

[a] College of Landscape Architecture, Nanjing Forestry University, Nanjing, 210037, PR China
[b] School of Tourism and Urban-Rural Planning, Zhejiang Gongshang University, Hangzhou, 310018, PR China
[c] University of Texas San Antonio, School of Architecture & Planning, San Antonio, TX, 78249, USA
[d] State Key Laboratory of Earth Surface Processes and Resource Ecology (ESPRE), Beijing Normal University, Beijing, 100875, PR China
[e] School of Architecture, Tsinghua University, Beijing, 100084, PR China

ARTICLE INFO

Keywords:
Urban thermal environment
LCZ
Demolition for Green
Urban heat island
Green ring

ABSTRACT

Urbanization combined with climate change has intensified the extreme heatwaves, especially in cities. To improve urban thermal environment, policymakers and urban planners have taken measures, such as plant more trees and design more green spaces. However, under the context of urbanization, the large scale of "demolition for green" policy rarely appeared in global cities. Therefore, the impact of "demolition for green" policy on urban thermal environments did not well uncovered. This study aims to address this gap by examining the "Demolition for Green" policy in Beijing, China, between 2000 and 2020. The Local Climate Zones (LCZ) classification and remote sensing data were applied to assess the effectiveness of this policy in mitigating the urban heat island (UHI) effect. The findings demonstrate that "Demolition for Green" policy can effectively improve the thermal environment in specific areas, as 56.02 % of those demolition areas transformed from the heat island to cool island, and this cooling effect are more efficient in urban central areas. However, this positive effect only existing in small areas of the city, it cannot offset the negative thermal effects brought by high-intensity construction and urban expansion, as the heat island area increased 148.12 km^2 in Beijing Sixth ring-road, and the average intensify of surface urban heat island (SUHI) increased from 0.98 °C (2000) to 1.61 °C (2020). The results highlight that besides the policy promotions, planning design measures should also be elaborated in urban development, thus helping the cities cope with climate change.

1. Introduction

In recent years, heatwaves have become more intense, frequent, and prolonged, and these trends are worsening due to global warming (Arsad et al., 2022). Rising urban air temperatures, driven by climate change and the urban heat island (UHI) effect, pose a serious risk to human health, as seen in increased mortality rates during heatwaves in cities worldwide (Iungman et al., 2023). For example, in 2019, due to high temperatures, global deaths exceeded 300,000, nearly 100,000 more than in 1990 (Ebi et al., 2021). In 2022, approximately 61,672 heat-related deaths occurred in Europe (Ballester et al., 2023). Therefore, it is urgent need to uncover the mechanism of UHI, and reduce the UHI effect to mitigate the adverse impacts of heat hazards on human well-being.

Previous studies focus on two aspects of UHI: air UHI (AUHI) associated with air temperature, and surface UHI (SUHI) associated with the Land Surface Temperatures (LST), the later has gained increasing attention due to its ease of access and a high spatial resolution (Du et al., 2016). SUHI is defined as urban surface temperature are higher than its surrounding rural areas (Geletič et al., 2019). Key factors influencing SUHI include land cover changes, anthropogenic activities, and others (Jabbar et al., 2023). Urban expansion, along with increased impervious surfaces like concrete and asphalt and reduced vegetation, alters surface energy, raising LST and intensifying the impact of SUHI (L. Chen et al.,

* Corresponding author at: School of Tourism and Urban-Rural Planning, Zhejiang Gongshang University, Hangzhou, 310018, PR China.
** Corresponding author at: University of Texas San Antonio, School of Architecture & Planning, San Antonio, TX, 78249, USA.
E-mail addresses: czhi0911@gmail.com (Z. Cai), huangyanlin2010@163.com (H. Huang).
[1] These authors contribute equally to this work and should be considered co-first authors.

https://doi.org/10.1016/j.scs.2025.106576
Received 24 January 2025; Received in revised form 23 June 2025; Accepted 24 June 2025
Available online 25 June 2025
2210-6707/© 2025 Elsevier Ltd. All rights are reserved, including those for text and data mining, AI training, and similar technologies.

2023; Ma et al., 2023; Moazzam & Lee, 2024; L. Zhao et al., 2018). Several studies have used various indicators such as building coverage, building height, building volume density, and frontal area index to examine the impacts of two-dimensional (2D) and three-dimensional (3D) urban morphologies on UHIs (Huang & Wang, 2019; Liao et al., 2021).These studies reveal that the geometric configuration of urban buildings affects wind flow, energy absorption and emission, which prompting further studies into 3D aspects (Han et al., 2023; Shao et al., 2023).

SUHI mitigation strategies focus on lowering temperatures in urban areas and enhancing human thermal resilience. Key approaches include urban greening, water management, urban ventilation, and controlling urban expansion (Deilami et al., 2018; Dutta et al., 2021). Extensive studies have shown that green spaces are the most effective strategy for mitigating UHI, mainly through evapotranspiration and shading (Wei et al., 2025; Y. Wu et al., 2025; Zhang et al., 2025). Green spaces, including green roofs, green facades, and parkland expansion, are recognized as effective urban heat mitigation measures (Besir & Cuce, 2018). The size and shape of green spaces also strongly influence their cooling effectiveness, with regular shapes like squares or circles providing greater efficiency than complex shapes (Liao et al., 2023; Y. Wu et al., 2025). To enhance climate resilience and mitigate UHI, several cities have launched urban greening projects. For instance, Shanghai's "Ecological Corridor" builds green corridors along rivers and roads, while New York City's "Million Trees NYC" aims to plant over one million trees to increase green coverage and mitigate UHI.

Although green spaces are widely acknowledged as effective in mitigating SUHI, previous studies have three main limitations: 1) Urbanization context: most cities are still urbanizing, with few implementing large-scale "Demolition for Green" policies. Consequently, research mainly focuses on the negative impacts of urbanization on SUHI, with limited attention given to the policy's role in improving the thermal environment (Rizvi et al., 2020). 2) Research perspective and methodology: While some studies have explored the relationship between 3D urban morphology and thermal effects, they often fail to address how urban renewal policies, such as "Demolition for Green" which require a detailed classification of urban morphology, can specifically influence thermal environments. Existing methods, which primarily focus on the static aspects of urban morphology or simple land use and built-up area classifications, do not fully capture the dynamic changes associated with urban renewal efforts and their impact on thermal conditions (Moazzam et al., 2022). 3) Temporal scale and climate adaptability: thermal environments are influenced by multiple factors. Focusing only on short-term effects may overlook the impacts of extreme weather events, highlighting the importance of considering the long-term dynamic effects of green spaces (Sheng et al., 2025).

To address these limitations, this study adopts the Local Climate Zone (LCZ) classification system, proposed by Oke and Stewart (2012), to categorize urban morphology and analyze the thermal environment. LCZ has demonstrated its effectiveness in thermal environment research, with numerous studies using LST to investigate SUHI across different urban regions (Tang et al., 2023; Yang et al., 2020). In recent years, the LCZ scheme has also been applied to urban morphology studies. For example, Cai (2022) utilized the LCZ scheme to analyzed the spatio-temporal transformation of 3D urban morphology across different cities, revealing three dynamic LCZ density patterns: spreading, shrinking, and relocation. Moreover, the integrating of LCZ into UHI analysis enables a deeper investigation of how urban morphology and land use influence LST and SUHI patterns, offering a fresh perspective for urban planning. Therefore, this study employs LCZ to capture urban morphological characteristics and quantify their thermal environment differences.

In recent years, Beijing has implemented two key urban development strategies: "reduction-based development" and "Demolition for Green." The former focuses on controlling urban land use and reducing inefficient built-up areas, while the latter aims to remove outdated buildings and expand green spaces to enhance the urban environment. The concept and implementation of "Demolition for Green" are formally embedded within Beijing's binding planning frameworks, as outlined in the Beijing Urban Master Plan (2004–2020) and the Beijing Green Space System Special Plan (2017–2035). These documents explicitly adopt the "Demolition for Green" approach to transform inefficient land into permanent green spaces, directly supporting the city's broader goals of mitigating urban sprawl, enhancing ecosystem services, and improving the urban thermal environment. This strategy is operationally integrated within Beijing's spatial governance system. For instance, the 2023 Greenway Special Plan prioritizes converting fragmented built-up areas into interconnected ecological corridors. Furthermore, the Beijing "14th Five-Year" Major Infrastructure Development Plan (The People's Government of Beijing Municipality, 2022) extends this approach by repurposing transportation spaces to promote low-carbon mobility.

In comparison, Shanghai's "Ecological Corridor" focuses on the Huangpu River waterfront greenway, limiting its urban coverage, while New York City's "Million Trees NYC" policy promotes tree planting but requires more comprehensive implementation to improve street greening. Similarly, the London Green Belt, which spans 500,000 hectares (22 % of the city), restricts urban sprawl, but it primarily works through land use regulation rather than active green infrastructure development (Amati & Yokohari, 2006). In Singapore, the Green Plan 2030 aims to develop 130 hectares of new parks and improve 170 hectares of existing ones (Liu et al., 2025). While the plan is a significant effort, it places some emphasis on technological solutions but does not solely rely on them to achieve its goals. In Medellín, the 46-mile-long Metropolitan Green Belt (Cinturón Verde), launched in 2012, integrates water protection, reforestation, urban greening, and congestion alleviation, while prioritizing social equity and climate-resilient development in poorer neighborhoods (Chu et al., 2017). In contrast, Beijing's "Demolition for Green" policy restructures the urban layout through large-scale green space restoration and a longer implementation period, offering a valuable case for studying its environmental impacts.

This study comprehensively examines the impact of the "Demolition for Green" policy on Beijing's thermal environment, aiming to address the following two questions:

1) How does the "Demolition for Green" areas impact the urban thermal environment, particularly in terms of mitigating heat island effects?
2) To what extent can the "Demolition for Green" policy offset the negative impacts of urban expansion on the UHI effect?

Thus, this study offers scientific insights for urban planners and policymakers to manage thermal environment and promote sustainable urban development.

2. Data and methods

2.1. Study area

Beijing, the capital of China, has experienced rapid urbanization, resulting in an expanded urban area and increasing concentrations of buildings and population (Fig. 1). From 2000 to 2020, Beijing's population increased from 13.64 million to 21.89 million (Beijing Municipal Bureau of Statistics, 2021), while the urban built-up area within the Sixth Ring Road expanded from 1001 km^2 to 1191 km^2. These developments have intensified the urban heat island (UHI) effect, exacerbating Beijing's thermal environment, with the hourly maximum UHI intensity reaching up to 8.4 °C during heatwave periods (Liu et al., 2020; Meng et al., 2023). Heatwaves and UHIs have significantly impacted human activities and labor productivity, contributing to a 3.5–10.2 % increase in deaths from cardiovascular diseases in Beijing (Qiang & Hu, 2022; Ren et al., 2021), underscoring the urgency of UHI mitigation for the city.

Besides the deterioration of the urban thermal environment, Beijing has also faced challenges such as land resource scarcity and

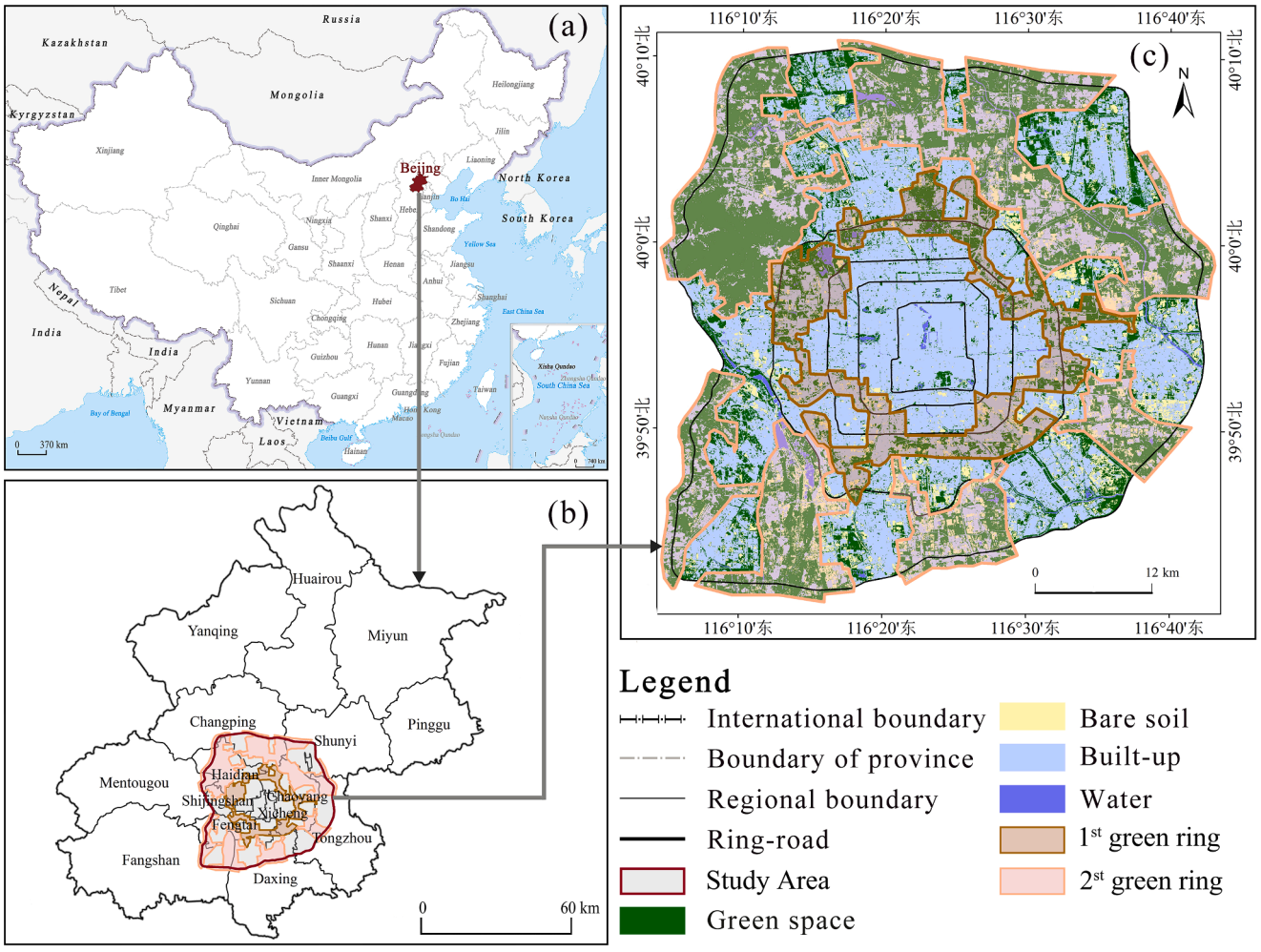


Fig. 1. The study area.

environmental degradation. To alleviate these issues, Beijing began experimenting with green separation belts in the 1990s. However, the policies during this period were relatively unsystematic, and "Demolition for Green" was not a central focus. Starting in 2000, the goal of a "Green Olympics" spurred the reinitiation of green separation belt projects (Tu et al., 2023). Between 2000 and 2004, Beijing reinforced the construction of green separation areas through the "Beijing Green Separation Area Special Plan," promoting land exchange and reclamation. The "Beijing Master Plan (2016–2035)" clearly defined "leave space to increase green" as a core goal to improve the urban ecological environment. "Demolition for Green" became a critical strategy for reducing urban expansion and optimizing ecological spaces (L. Zhou et al., 2024). In 2017, Beijing demolished nearly 60 million square meters of illegal construction, and in 2018, it proposed reclaiming land for greening, planning to convert 1600 hectares into green corridors and urban leisure parks (Chinese Government, 2018). Currently, Beijing's "Demolition for Green" policy has entered a more refined management stage. Although this policy has led to many positive outcomes, there remains a research gap regarding its effects on the urban thermal environment.

2.2. Data sources

For LCZ sample labeling, super-high-resolution (SHR) imagery from the Google series was used for the labeling layer, while multi-band imagery from the Sentinel and Landsat series served as the classification layer. Since SHR imagery has only been available after 2000 and spatial changes take time to manifest, 2000 was chosen as the starting point and analyze Beijing's urban morphology and green space at five-year intervals. To enhance sample labeling accuracy, remote sensing satellite images for the target year and images from the six months before and after each period, were included. Furthermore, to avoid the impact of snow cover on ground observation during winter, data from December to February were excluded.

To obtain temperature change data, Landsat series remote sensing images were downloaded from the USGS website. Although Landsat data has relatively lower spatial resolution compared to newer satellite imagery, its long-term temporal coverage and consistency provide a unique advantage, especially for monitoring urban temperature changes over extended periods. The satellite data, recorded around 10:30 AM (Beijing time), included images from the following dates: August 20, 2000; July 25, 2005; August 8, 2010; August 22, 2015; and August 3, 2020. These dates were selected because they coincide with periods of minimal cloud cover during the summer months of the target years. To address potential issues related to cloud cover, additional images from June to September of the preceding and subsequent years were also used for error assessment and data correction. For example, for the year 2000, images from August 10, 1999, July 14, 2001, and August 31, 2001, were used as reference data to correct areas affected by cloud cover. This approach ensured that the thermal measurements were as accurate as possible by mitigating the impact of cloud cover on the data.

2.3. Methods

The methodology contains three parts: LCZ classification and green spaces identification, thermal environment analysis, and mechanism analysis (Fig. 2). 1) LCZ classification and green spaces identification: Using ArcGIS 10.4 software and LCZ Generator platform, urban areas and its surrounding rural areas were classified into two categories (built-up and nature landcover) and 15 LCZ classes with five-year intervals, where the nature landcover category were mainly used to identify urban green spaces. 2) Thermal environment analysis. ArcGIS and ENVI software were employed to calculate LST and SUHI, followed by a spatio-temporal evolution analysis of these parameters. 3) Mechanism analysis. The relationship between SUHI and LCZ was explored to understand the impact of "Demolition for Green" policy on the thermal environment.

2.3.1. LCZ classification and "Demolition for Green" areas identification

2.3.1.1. (1) LCZ classification. The generation of the LCZ map involves three main steps: sample labeling, machine learning classification, and evaluation feedback. This process not only categorizes urban morphology into built-up and natural land cover but also provides detailed differentiation of urban green spaces.

Step 1: Sample Labeling. Based on satellite imagery from different periods, manual visual interpretation was used to label samples for various LCZ classes within the study area. A total of 17,131 samples were labeled during this phase.
Step 2: Machine Learning Classification. The labeled samples were uploaded to Google Earth Engine (GEE), utilizing its extensive image database and powerful data processing capabilities. The machine learning algorithm and code were improved based on the LCZ Generator (http://lcz-generator.rub.de) (Demuzere et al., 2021).

Step 3: Accuracy Evaluation and Correction. The standard cross-validation methods were used for accuracy assessment. Based on the classified LCZ map, 30 % of the samples that were not part of the classification was randomly selected, for accuracy evaluation. The accuracy evaluation results indicate that most LCZ classes achieved an overall accuracy rate of over 65 %, with an overall weighted accuracy of approximately 90 % (The weighted accuracy treats similar morphological zones as a whole, assigning higher weight to them during the accuracy assessment. For example, high-density high-rise, mid-rise, and low-rise can be considered as a group, while low-density high-rise, mid-rise, and low-rise can be grouped together as another.). For relatively simple types, such as green spaces and water, the classification accuracy exceeded 85 %, meeting the machine learning requirement of a minimum accuracy level of 0.5 (Bechtel et al., 2019). To further improve the accuracy of morphological classification, the study used existing road and vector building data, applying threshold values to classify spatial morphology. These classifications were then used as references for manually correcting some of the machine classification results.

2.3.1.2. (2) the identification of green spaces. The LCZ classified urban morphology into two main categories: built-up and natural land cover. Each LCZ class is associated with 10 indicators related to the thermal environment. These indicators are based on previous research, data measurements, and comprehensive experiential value. Using these indicators, built-up is classified into 10 subcategories, while natural land cover is divided into 7 subcategories.

The identification of urban green spaces is primarily based on natural land cover categories within the LCZ framework—specifically dense trees (LCZ-A), scattered trees (LCZ-B), and low plants (LCZ-D). Distinguishing between these green space types is a crucial part of the analysis, yet it presents certain challenges. For example, LCZ-B and LCZ-D, while both representing green spaces, can exhibit significant overlap

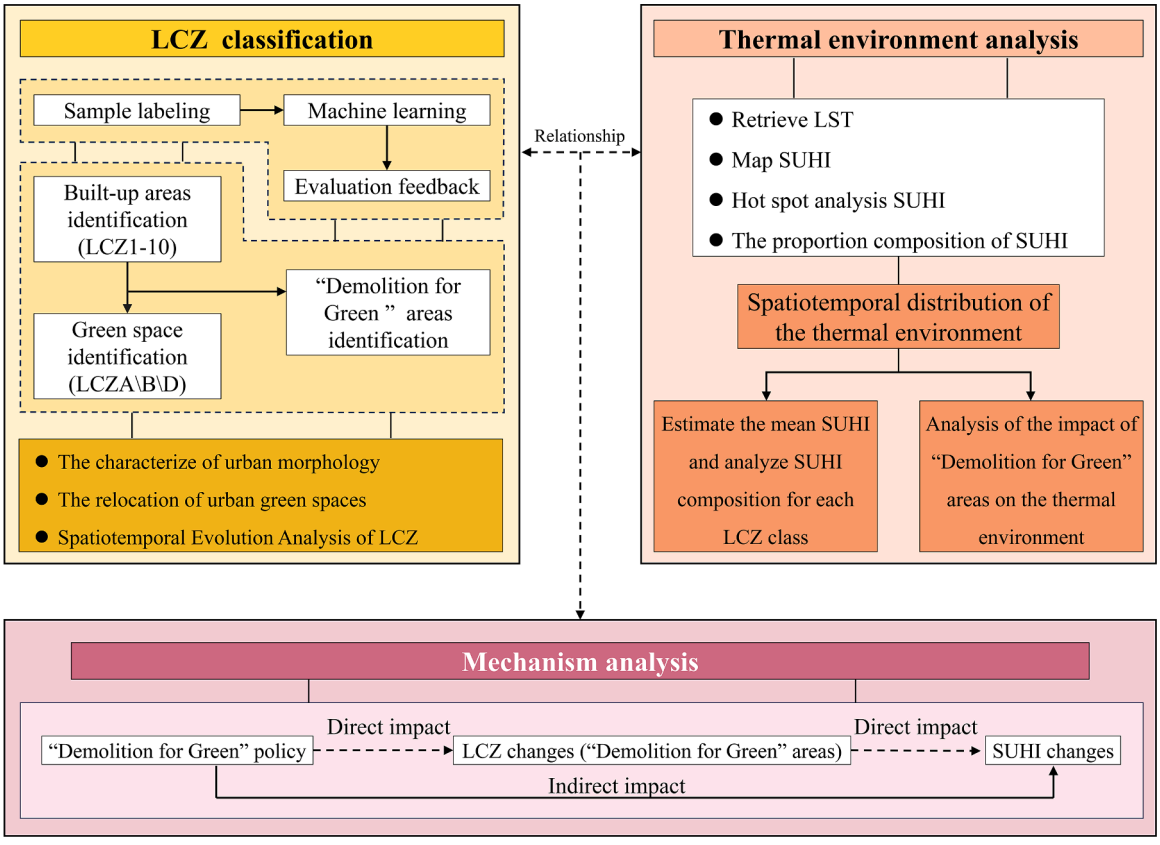


Fig. 2. The workflow of the study methodology.

in their physical characteristics, making it difficult to differentiate between the two. To address this, five key parameters were analyzed in detail (see Table 1): Tree Aspect Ratio (TAR), Impervious Surface Fraction (ISF), Mean Plant Height (MPH), Sky View Factor (SVF), and Terrain Roughness Class (TRC). The choice of these parameters is supported by previous studies that have linked these metrics to the thermal and ecological performance of urban green spaces.

2.3.1.3. (3) the identification of built-up areas. The identification of built-up areas is primarily based on built-up categories. For built-up areas, where traditional vegetation metrics are not applicable, Canyon Aspect Ratio (CAR) and Building Aspect Ratio (BAR) were used in place of TAR, and Mean Building Height (MBH) replaced MPH. The parameter values for each LCZ class are provided in Table 1. This expanded set of parameters not only justifies the selection of specific LCZ classes and thresholds but also enhances the overall accuracy of the LCZ classification by capturing a broader spectrum of urban features.

In this study, certain LCZ classes, such as lightweight low-rise (LCZ-7) and bush and scrub (LCZ-C), were excluded. Specifically, LCZ-7 typically refers to compact, single-story buildings constructed with lightweight materials and is generally associated with informal settlements, while LCZ-C represents desert shrub or scrubland. Given Beijing's rapid urbanization, where available land is scarce, the distribution of LCZ-C is minimal or even absent. Moreover, as the capital of China, Beijing's economic development level is relatively high, and lightweight constructions are uncommon. Consequently, excluding LCZ-7 and LCZ-C in this study aligns with Beijing's actual urban conditions. Some scholars have also omitted LCZ-7 and LCZ-C from the LCZ classification for Beijing (Liu et al., 2024; Yin & Zhao, 2024).

2.3.1.4. (4) the identification of "Demolition for Green" areas. The "Demolition for Green" areas refer to those originally identified as built-up areas in the base year, which are transformed into green spaces as part of the urban renewal process in the target year. In this process, special attention must be given to the spatial transformation between these green spaces and the existing built-up areas.

Table 1
LCZ classification class.

	LCZ classes	CAR	ISF (%)	MBH (m)	SVF	TRC
Built-up	Compact high-rise (LCZ-1)	> 2	40 - 60	> 25	0.2 - 0.4	8
	Compact mid-rise (LCZ-2)	0.75 - 2	30 - 50	10 - 25	0.3 - 0.6	6 - 7
	Compact low-rise (LCZ-3)	0.75 - 1.5	20 - 50	3 - 10	0.2 - 0.6	6
	Open high-rise (LCZ-4)	0.75 - 1.25	30 - 40	> 25	0.5 - 0.7	7 - 8
	Open mid-rise (LCZ-5)	0.3 - 0.75	30 - 50	10 - 25	0.5 - 0.8	5 - 6
	Open low-rise (LCZ-6)	0.3 - 0.75	20 - 50	3 - 10	0.6 - 0.9	5 - 6
		BAR	**ISF (%)**	**MBH (m)**	**SVF**	**TRC**
	Large low-rise (LCZ-8)	0.1 - 0.3	40 - 50	3 - 10	> 0.7	5
	Sparsely built (LCZ-9)	0.1 - 0.25	< 20	3 - 10	> 0.8	5 - 6
	Heavy industry (LCZ-10)	0.2 – 0.5	20 – 40	5 - 15	0.6 – 0.9	5 - 6
		TAR	**ISF (%)**	**MPH (m)**	**SVF**	**TRC**
Nature land cover	Dense trees (LCZ-A)	> 1	< 10	3 - 30^{+}	< 0.4	8
	Scattered trees (LCZ-B)	0.25 - 0.75	< 10	3 - 15	0.5 - 0.8	5 - 6
	Low plants (LCZ-D)	< 0.1	< 10	< 1	> 0.9	3 - 4
	Bare rock or paved (LCZ-E)	< 0.1	> 90	< 0.25	> 0.9	1 - 2
	Bare soil or sand (LCZ-F)	< 0.1	< 10	< 0.25	> 0.9	1 - 2
	Water (LCZ-G)	< 0.1	< 10	< 0.25	> 0.9	1

2.3.2. Thermal environment analysis

2.3.2.1. (1) the retrieve of LST. Landsat series remote sensing images from five different years (2000, 2005, 2010, 2015, and 2020) were used to retrieve the LST values with ENVI 5.6.2. The temperature data were normalized and used the average values across multiple periods were used as representative values. The normalization formula is:

$$NLST_i = \frac{LST_i - LST_{min}}{LST_{max} - LST_{min}} \tag{1}$$

Where $NLST_i$ is the normalized surface temperature value for image i; LST_i is the actual surface temperature value for image i, and LST_{max} and LST_{min} are the maximum and minimum surface temperatures in the study area, respectively.

The Radiative transfer equation (RTE) was applied to retrieve the LST from radiance, selecting only TIRS Band 10. Combined with the spectral response function of TIR channel, the radiance received by the sensor (L_{obs}) is recognized as the sum of three parts: the upward atmospheric thermal radiance (L_u), the downward atmospheric thermal radiance (L_d) reflected by the surface and the radiance emitted directly from surface (ε) (Li et al., 2023).

$$L_{obs} = (L_T\varepsilon + (1-\varepsilon)L_d)\tau + L_u \tag{2}$$

Where L_T represents the blackbody radiance, τ is the atmospheric transmittance. According to Eq. (2), L_T can be expressed as:

$$L_T = \frac{L_{obs} - L_u - \tau(1-\varepsilon)L_d}{\tau\varepsilon} \tag{3}$$

ε can be expressed as:

$$\varepsilon = \begin{cases} 0.979 - 0.046_{\rho R} & NDVI < 0.2 \\ 0.987P_V + 0.971(1-P_V) + d\varepsilon & 0.2 \le NDVI \le 0.5 \\ 0.987 + d\varepsilon & NDVI > 0.5 \end{cases} \tag{4}$$

Where ρR is the reflectance value of the red band, $d\varepsilon$ is the cavity effect and regarded as 0 for flat surfaces, P_V is the vegetation fraction. Using the Planck formula, the target temperature T_s can be calculated:

$$T_S = \frac{K_2}{\ln\left(\frac{K_1}{L_T} + 1\right)} \tag{5}$$

The values of K_1 and K_2 can extracted from the Landsat metadata, and LST (°C) can be calculated as follow equation:

$$LST = T_S - 273.15 \tag{6}$$

2.3.2.2. (2) definition and classification of SUHI. As urban areas expand, the boundary between urban and rural zones becomes increasingly blurred, complicating the definition of these areas. In this study, measurement points were selected based on the natural land cover classes within LCZ-A, B, D, and F. A 200-meter buffer zone was created around each measurement point, and the average temperature within this buffer was used as the background temperature. To eliminate the topographical bias, areas with elevation exceeding 50 m and any water bodies within the buffer were excluded (C. Zhao et al., 2024). Several studies have previously used buffer zones to calculate SUHI (Wang et al., 2022; Yang et al., 2023). Our approach, which uses a 200-meter buffer, better reflects the influence of surrounding vegetation and land use, as research has shown that the influence of SUHI can extend up to 200 m (Liang et al., 2022). Furthermore, factors like tree, shrub, and grass coverage within 200 m, as well as larger green spaces (≥2 ha), are known to have cooling effects, which are integrated into this method to

provide more accurate SUHI calculations (Johnson et al., 2020), as well as the presence of green spaces, with larger green spaces (≥2 ha) cooling the surrounding areas by up to 2 °C, particularly at distances between 50 and 200 m (Lemoine-Rodríguez et al., 2022). This supports the choice of a 200-meter buffer zone for more accurate SUHI calculations. To further minimize the impact of weather variations, SUHI is used as a comparative indicator, and the study area is categorized into five temperature zones: CI (cool island), WHI (weak heat island), MHI (moderate heat island), SHI (strong heat island), and EHI (extreme heat island). The specific classification criteria are shown in Table 2.

2.3.2.3. (3) urban LST hotspot analysis. To supplement the LCZ classification, this study employed hotspot analysis to assess urban pixel heterogeneity. Urban LST hotspots, representing the most heat-intensive areas, are defined as pixels with temperatures exceeding two standard deviations above the area's mean. The analysis was conducted using the ArcGIS 10.4 platform, and hotspot detection was calculated as follows (Portela et al., 2020):

$$LST > \mu + 2 \times \delta \tag{7}$$

Where μ and δ respectively stand for the average and standard deviation of LST in the study area.

2.3.3. Mechanism analysis

To thoroughly explore the impact of the "Demolition for Green" policy on urban thermal environments, this study analyzes two key aspects: the changes in urban spatial morphology and the mechanisms of thermal environment interaction. First, based on the LCZ system and integrating remote sensing imagery with GIS technology, the study categorizes the climate types of the study area. It further analyzes the evolution of these areas in the context of urban spatial patterns, revealing the transformation of built-up land into green spaces under the "Demolition for Green" policy. Next, the study examines surface temperature data from different years to identify heat island areas, focusing on the changes in the SUHI in areas where built-up land has transitioned into green spaces and their surrounding regions. Overall, it reveals the dynamic characteristics of the thermal environment before and after the implementation of the "Demolition for Green" policy in these areas.

3. Results

3.1. The transformation of urban morphology

3.1.1. The characterize of urban morphology

From 2000 to 2020, Beijing's urban morphology and spatial layout within the Sixth Ring Road underwent great changes (Fig. 3). In terms of land use, built-up expanded, reflecting a pattern of high-intensity development spreading outward from the center. Local Climate Zones (LCZ) compositions shifted from compact to more open classes.

As shown in Fig. 4(a), during urban expansion, low-rise classes (LCZ-3, LCZ-6) exhibited a significant decline, while high-rise classes (LCZ-1, LCZ-4) showed a substantial growth, with dramatic land use changing, particularly between 2010 and 2020. Mid-rise classes (LCZ-2, LCZ-5) and large low-rise class (LCZ-8) experienced relatively minor changes. Compact classes (LCZ-1, LCZ-2, LCZ-3) generally decreased, whereas open classes (LCZ-4, LCZ-5, LCZ-6) showed an increasing trend.

Table 2
Five temperature zones.

SUHI intensity levels	Classification criteria
CI	SUHI ≤ 0
WHI	0<SUHI ≤ 2
MHI	2<SUHI ≤ 4
SHI	4<SUHI ≤ 7
EHI	7<SUHI

For land use analysis, the 15 LCZ classes were classified into five categories: built-up, greenspace, paved, bare soil, and water, as shown in Fig. 4(b). In 2000, the built-up and greenspace areas within Beijing's Sixth Ring Road were roughly equivalent. After 2000, built-up areas surpassed greenspace and showed an overall increasing trend. However, after 2015, built-up areas began to decrease. Water area changed slightly, paved areas saw relatively minor overall changes, whereas bare soil rapidly decreased between 2010 and 2015, then rebounded quickly.

Detailed analysis of each LCZ class, as shown in Fig. 4(c), reveals that compact high-rise (LCZ-1) and open high-rise (LCZ-4) experienced the most significant growth, increasing from 2.0 %, 0.3 % in 2000 to 7.5 %, 10.1 % in 2020, respectively. Compact mid-rise (LCZ-2) and open low-rise (LCZ-6) also shows an upward trend. In contrast, compact low-rise (LCZ-3) experienced a marked decline, decreasing from 21.0 % (2000) to 7.5 % (2020). Large low-rise (LCZ-8) initial grew from 4.9 % (2000) to 11.0 % (2015), then fell to 7.8 % (2020). Other classes showed small changes. Additionally, the distribution of built-up classes became more balanced over time. As LCZ-3 decreased and other LCZ classes expanded, by 2020, the land use proportions for LCZ 1–5 ranged from 7 % and 10 %.

In terms of spatial layout, the distribution of various LCZ classes shifted from a dispersed pattern to a compact arrangement, with built-up classes spreading outward. The increase built-up land was particularly notable in the peripheral areas, with construction intensity gradually rising, as shown in Figs. 3 and 5. In 2000, LCZ-2 was the predominant built-up class within the Third Ring Road, accounting for over 40 %, while LCZ-3 dominated the area between the Third and Sixth Ring Roads, comprising approximately 50 %. By 2020, the proportions of LCZ-1 and LCZ-4 had risen significantly across all rings. However, LCZ-2 remained the main built-up class within the Fourth Ring, making up over 30 % while beyond the Fourth Ring, LCZ-4 held a larger share, around 20 %. From 2000 to 2015, the proportion of LCZ-8 steadily increased, particularly in the area between the Fourth and Sixth Rings, rising from 11 % to 23 %. However, after 2015, the proportion of LCZ-8 generally declined across all rings, with the most notable decrease between the Fourth and Fifth Rings. Among natural land-use types, LCZ-B, largely consisting of urban parks and green spaces, has shown an upward trend in area. Spatially, LCZ-B has increased within all rings, indicating that "Demolition for Green" activities are widespread throughout the city. Notably, the Fifth and Sixth Ring Roads experienced the largest LCZ-B growth, reflecting substantial greening or park development in these zones. Conversely, LCZ-D, mainly farmland, has shown a consistent decline in area.

3.1.2. The relocation of urban green spaces

The urban green spaces in this study primarily include dense trees (LCZ-A), scattered trees (LCZ-B), and low plants (LCZ-D). Urban green space exhibited a decreasing trend, particularly between 2000 and 2010. After 2010, greenspace change remained relatively stable. From a spatial layout perspective, urban green spaces were progressively encroached upon by built-up land, resulting in a gradual reduction and fragmentation of the total greenspace area. The greenspace type gradually shifted from LCZ-D to LCZ-B, indicating a qualitative improvement in greenspace to some extent. Urban green spaces became increasingly concentrated in the city center, while greenspace in peripheral areas was further reduced by expanding built-up areas.

Regarding the quantity of greenspace, as shown in Fig. 4, the proportion of green space within Beijing's Sixth Ring Road decreased from 45 % (2000) to 35 % (2020), following a wave-like pattern of initial decrease, slight increase, and subsequent decline. Specifically, LCZ-A showed an overall decreasing trend but with minimal fluctuations; LCZ-B exhibited a significant increase, with rapid growth particularly between 2010 and 2015; and LCZ-D experienced a rapid decline, with its area decreasing sharply from 2000 to 2020.

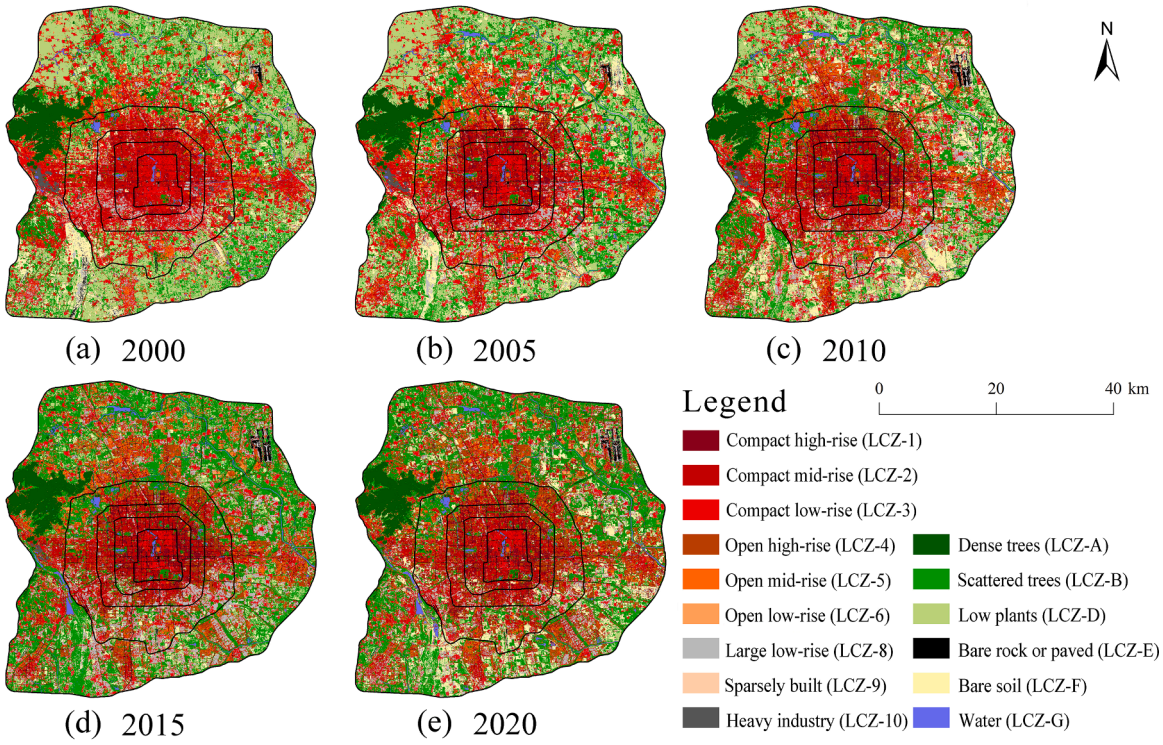


Fig. 3. LCZ Maps Obtained for (a) 2000, (b) 2005, (c) 2010, (d) 2015, (e) 2020.

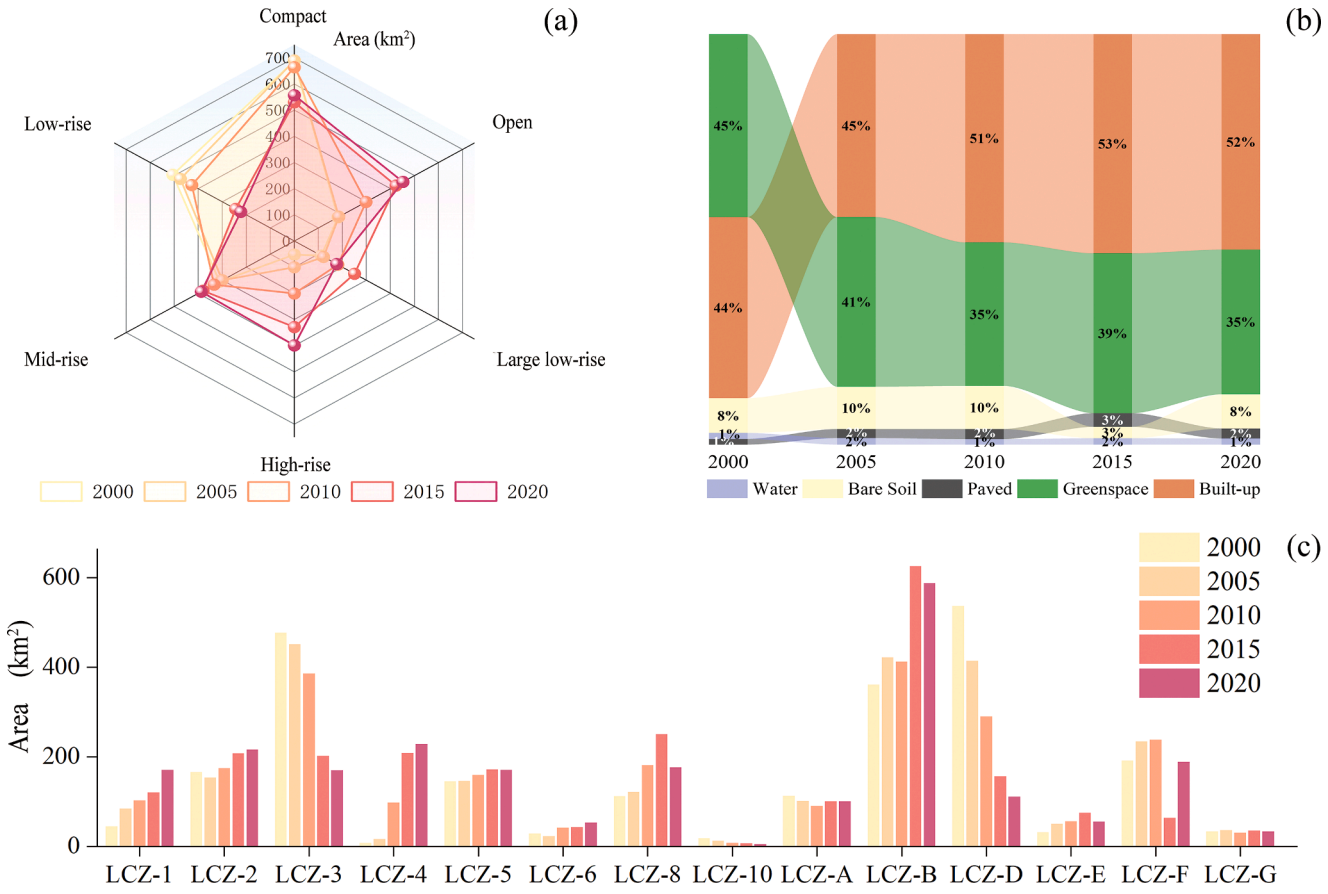


Fig. 4. Changes in (a) built-up classes, (b) LCZ classes, and (c) area of different LCZ classes from 2000 to 2020.

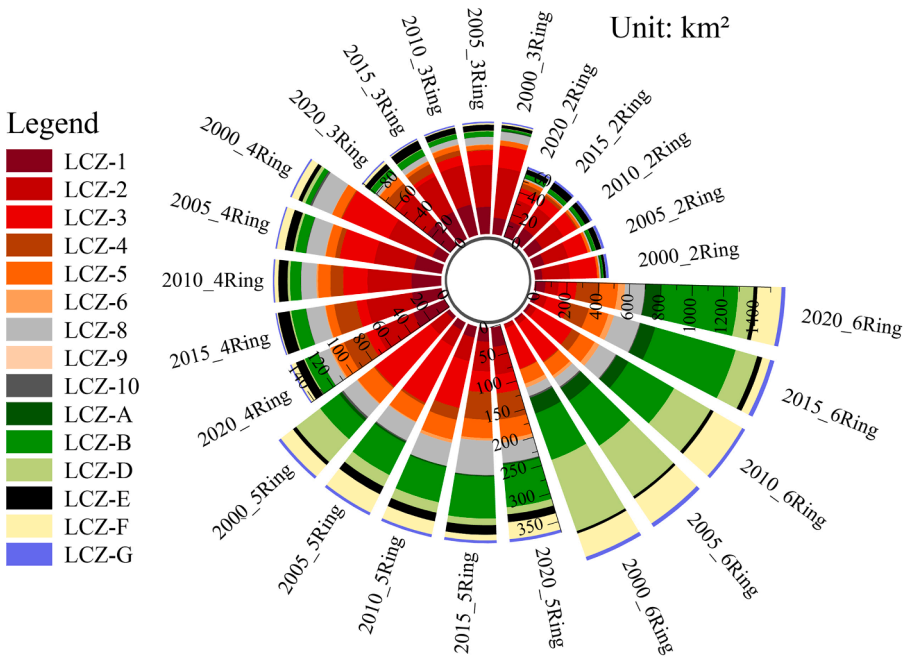


Fig. 5. Areas of LCZ classes across different ring road from 2000 to 2020.

3.1.3. Spatiotemporal evolution analysis of LCZ classes

From 2000 to 2020, both the quantity and spatial distribution of various LCZ classes underwent significant changes. To better analyze these trends, LCZ maps for different years were overlaid, as shown in Fig. 6. In terms of quantity, the built-up classes LCZ-1, LCZ-2, LCZ-4, and LCZ-8 showed notable increase. Specifically, LCZ-2 primarily transitioned from LCZ-3, LCZ-1 mainly transitioned from LCZ-2 and LCZ-4, LCZ-4 was mainly derived from LCZ-F and LCZ-12, and LCZ-8 mainly transitioned from LCZ-3. LCZ-3 experienced a significant reduction, particularly between 2010 and 2015, as it transitioned into LCZ-8 and LCZ-F. Other building types showed relatively minor changes. Among the natural types, LCZ-B and LCZ-D exhibited a substantial number of mutual transitions. However, after 2015, LCZ-D and LCZ-F mainly transitioned into LCZ-B. Additionally, a large portion of LCZ-D also shifted into LCZ-F, which then further transformed into other classes. LCZ classes were categorized into built-up, green spaces, water, paved,

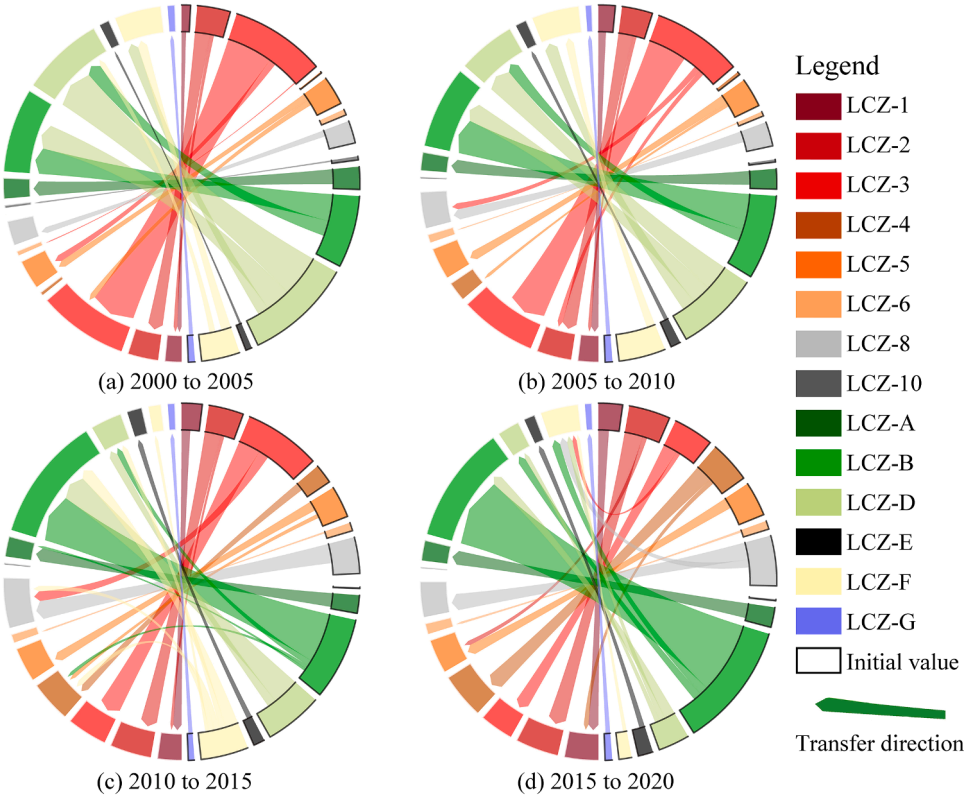


Fig. 6. Transition of LCZ classes from 2000 to 2020.

and bare soil, and the transitions between these types from 2000 to 2020 were analyzed. Detailed data can be found in Table 3. The most significant transitions occurred from green spaces to built-up areas, followed by the transition from built-up areas to green spaces.

3.2. Spatiotemporal changes in the urban thermal environment

3.2.1. Spatiotemporal distribution of the thermal environment

From 2000 to 2020, urban surface temperatures remained relatively high, forming a sharp contrast with surrounding areas of lower surface temperatures. The urban-rural gradient effect indicates that factors such as densely distributed buildings within cities, large-scale construction of impervious surfaces, polarization phenomena, frequent population activities, and the limited presence of urban green spaces and water are all key factors contributing to the gradual deterioration of the urban thermal environment.

As shown in Fig. 7(a), there was significant differentiation in NLST within the study area. From 2000 to 2015, the area with an NLST > 0.5 continuously expanded, but by 2020, this trend reversed, showing a decrease. The average LST of rural areas was calculated, and values exceeding this average were extracted, as shown in Fig. 7(b). Over time, the average LST in rural areas shows a gradual increase. Spatially, the UHI exhibited a trend of spreading outward from the city center; however, expansion was relatively limited in the northeastern and western regions. This was primarily due to the large mountainous areas in the west, which suppressed the formation, while in the northeast, airport restricted urban expansion. To further clarify the clustering patterns of LST within UHI areas, a hot and cold spot analysis was conducted to identify LST clustering types, as shown in Fig. 7(c). From 2000 to 2020, the extent of continuous hot spot areas increased, while cold spots gradually transformed into non-significant areas, indicating a deterioration of the urban thermal environment.

The spatial distribution of surface urban heat island (SUHI) within the study area is shown in Fig. 8. Cool Island (CI) were primarily located outside the Fifth Ring. From 2000 to 2005, the CI area increased, but after 2005, the cool island area began to steadily decrease. Meanwhile, the heat island area increased by 148.12 km^2 in the area inside the Sixth Ring Road, and the average intensity of SUHI rose from 0.98 °C (2000) to 1.61 °C (2020).

3.2.2. Analysis of the relationship between LCZ classes and the thermal environment

The relationship between SUHI and LCZ classes was analyzed using statistical methods, with a box plot illustrating annual average SUHI trends for different LCZ classes. As seen in Fig. 9, there are great differences in average SUHI among various LCZ classes from 2000 to 2020.

Overall, the SUHI of built-up classes (LCZ 1–10) was generally higher than that of natural land cover classes (LCZ A-G), indicating a stronger urban heat island effect in built-up areas compared to natural areas. Specifically, the average SUHI of compact classes was significantly higher than that of open classes, with an average difference of 2.0–3.0 °C. This is mainly due to high-density impervious surfaces and limited ventilation, which hinder effective heat dissipation (Xiang et al., 2022), significantly increasing SUHI. Moreover, among compact classes, low-rise class exhibit higher SUHI values (B. Chen et al., 2022; Guo et al., 2020; Yin et al., 2018). When comparing high-rise, mid-rise, and low-rise classes, SUHI follows a descending order: mid-rise, low-rise, and high-rise, with average SUHI values of 3.2 °C, 2.4 °C, and 1.9 °C, respectively. The characteristics of high-density areas include a greater proportion of hard surfaces, increased artificial heat emissions, reduced ventilation and cooling spaces, and higher surface temperatures. Additionally, the strong urban canyon effect leads to lower surface temperatures in high-rise areas. In contrast, low-rise buildings, lacking the shading effect and solar radiation barriers provided by taller buildings, exhibit higher SUHI than high-rise buildings in both compact and open urban morphology. This highlights the different impacts of building heights on the urban heat island effect.

Large low-rise (LCZ-8) exhibited relatively high SUHI among the built-up classes, especially during the period from 2000 to 2005, where it increased by 2.0 °C. This increase of SUHI in LCZ-8 is closely related to the growth of industrial and large commercial areas (Hu et al., 2020). These areas, with their vast building footprints and impervious surfaces, absorb and reflect substantial solar radiation, further elevating local SUHI. Similar trends have been observed in other cities, indicating that large-scale low-rise building areas often exert a more intense heat effect than anticipated. In contrast, sparsely built (LCZ-9) showed lower SUHI, likely due to the increase in green space. Heavy industrial (LCZ-10) had the highest SUHI, as heat sources and extensive impervious surfaces in this zone led to high albedo and elevated temperatures (Unal Cilek & Cilek, 2021).

Natural LCZ classes, due to their higher proportion of permeable surfaces, generally have lower SUHI values. Dense trees (LCZ-A) and water (LCZ-G) exhibited the lowest surface temperatures, particularly LCZ-A, where the tall vegetation and large leaf area effectively blocked solar radiation and released more heat through transpiration. The average SUHI of low plants (LCZ-D) were also low, though higher than that of LCZ-A and LCZ-B, primarily because low vegetation cannot sufficiently block solar radiation. Additionally, in 2020, the SUHI of LCZ-D was slightly above 0 °C, consistent with the overall stronger heat island effect observed that year. Over the past two decades, bare rock or paved (LCZ-E) consistently exhibited relatively high SUHI values, nearing those of built-up areas. The SUHI of bare soil (LCZ-F) falls between that of LCZ-D and LCZ-E.

To address the limitations of LCZ classifications in representing average surface temperature patterns over a large area, a gradient analysis was conducted. Over 150,000 evenly distributed data points were sampled, calculating the proportion of areas with varying SUHI intensities across LCZ classes (Fig. 10). Results revealed that compact classes (LCZ 1–3) had significantly higher SHI and EHI proportions compared to open LCZs, particularly for LCZ-4, where the proportion was below 10 %. LCZ-8 and LCZ-10 showed higher proportions of SHI and EHI, especially LCZ-10, where the proportion reached 80 % in 2020. Conversely, LCZ-G and LCZ-A displayed a strong cool island effect, contributing over 70 % to cooling areas. These findings highlight LCZ-specific impacts on both SUHI intensity and urban temperature patterns.

Table 3
Land cover type transition matrix from 2000 to 2020.

Land cover types		2020 Area (km^2)					
		Built-up	Greenspace	Paved	Bare Soil	Water	Total Transitions Out
2000 Area (km^2)	Built-up	755.95	143.38	29.86	66.30	5.56	1001.05
	Greenspace	324.46	573.44	12.48	94.29	6.15	1010.82
	Paved	14.11	4.70	10.26	2.10	0.38	31.55
	Bare Soil	86.86	71.71	2.50	24.41	6.58	192.07
	Water	9.28	6.49	0.39	2.04	15.03	33.23
	Total Transitions In	1190.66	799.72	55.49	189.15	33.71	2268.72

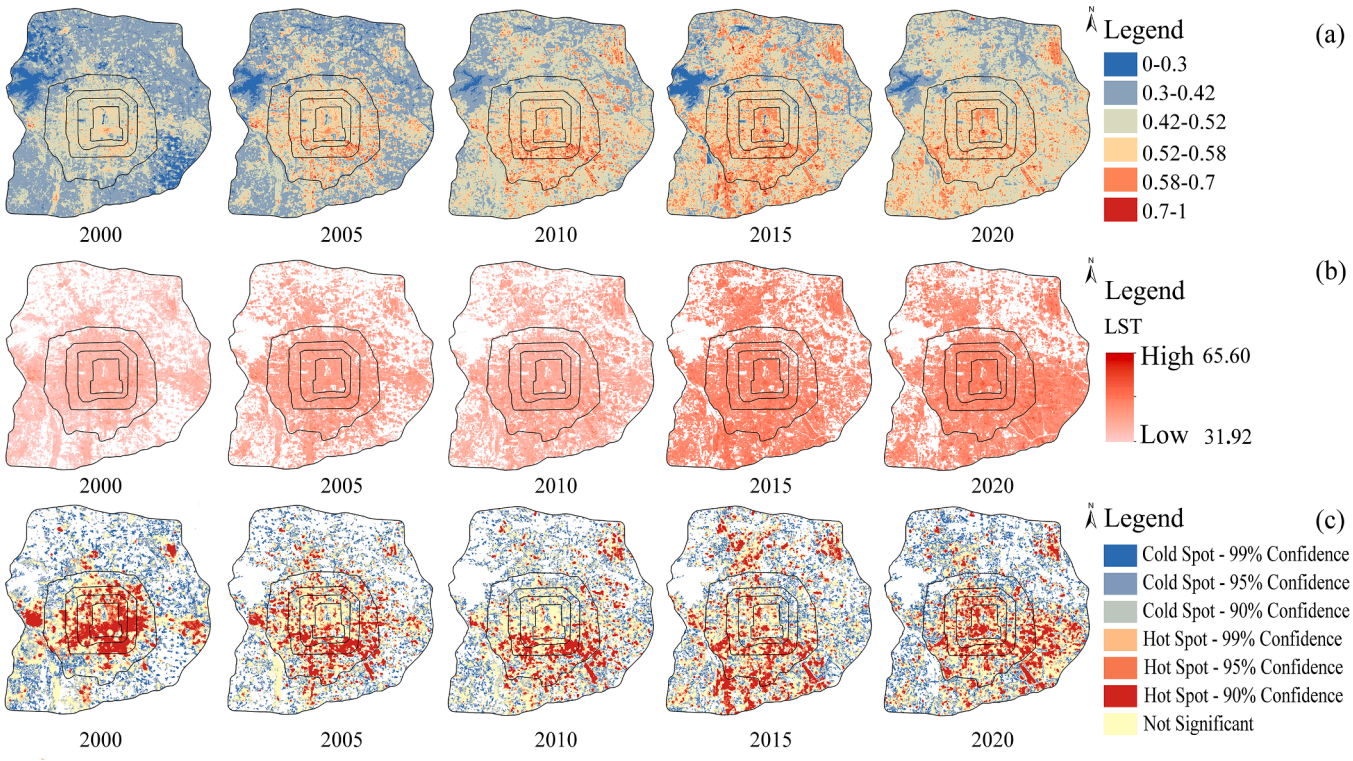


Fig. 7. (a) Normalized land surface temperature (NLST) distribution from 2000 to 2020; (b) Land Surface Temperatures (LST) distribution within the urban heat island (UHI) areas from 2000 to 2020. (c) Hotspot and coldspot distribution of LST within the UHI areas from 2000–2020.

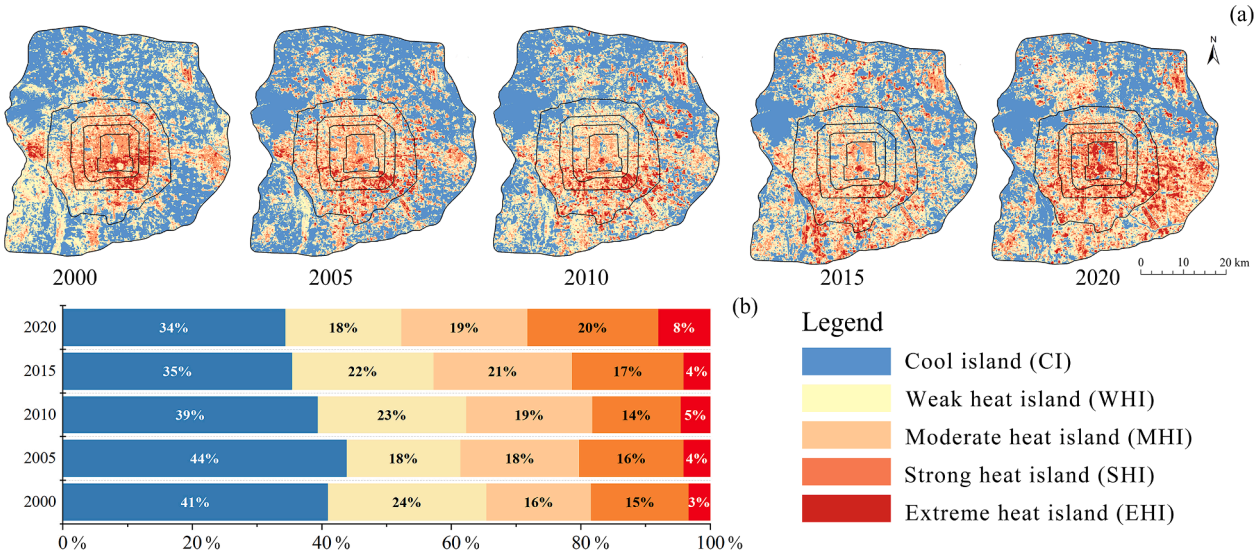


Fig. 8. (a) The spatial distribution and (b) proportion composition of SUHI from 2000 to 2020.

3.2.3. *Analysis of the impact of "Demolition for Green" policy on the thermal environment*

This study extracts and conducts a detailed analysis of the main types of LCZ conversions, which include the following six categories: bare soil to built-up, bare soil to greenspace, greenspace to bare soil, built-up to greenspace (i.e., "Demolition for Green"), built-up to bare soil, and greenspace to built-up. Based on the fitting analysis results of SUHI in 2000 and 2020 (Figs. 11(a, c), it was found that the SUHI in areas undergoing "Demolition for Green" significantly decreased from 2000 to 2020, with a slope of 0.44 and a p-value of <0.0001, indicating a significant cooling effect of the "Demolition for Green" policy on the thermal environment. Compared to other types of land-use conversions, the cooling effect of "Demolition for Green" was more pronounced.

To further validate the long-term thermal environmental effects of the "Demolition for Green" policy, a temporal analysis was conducted on the type conversion areas from 2000 to 2020, with a five-year interval (Figs. 11(b, c)). Throughout all time periods, the cooling effect in "Demolition for Green" areas remained significant ($P < 0.0001$). Between 2000 and 2005, the policy had a significant positive impact on the thermal environment. As this period marked an earlier stage of urbanization, the policy's implementation likely had a more pronounced effect on mitigating the urban heat island effect. The focus during this time

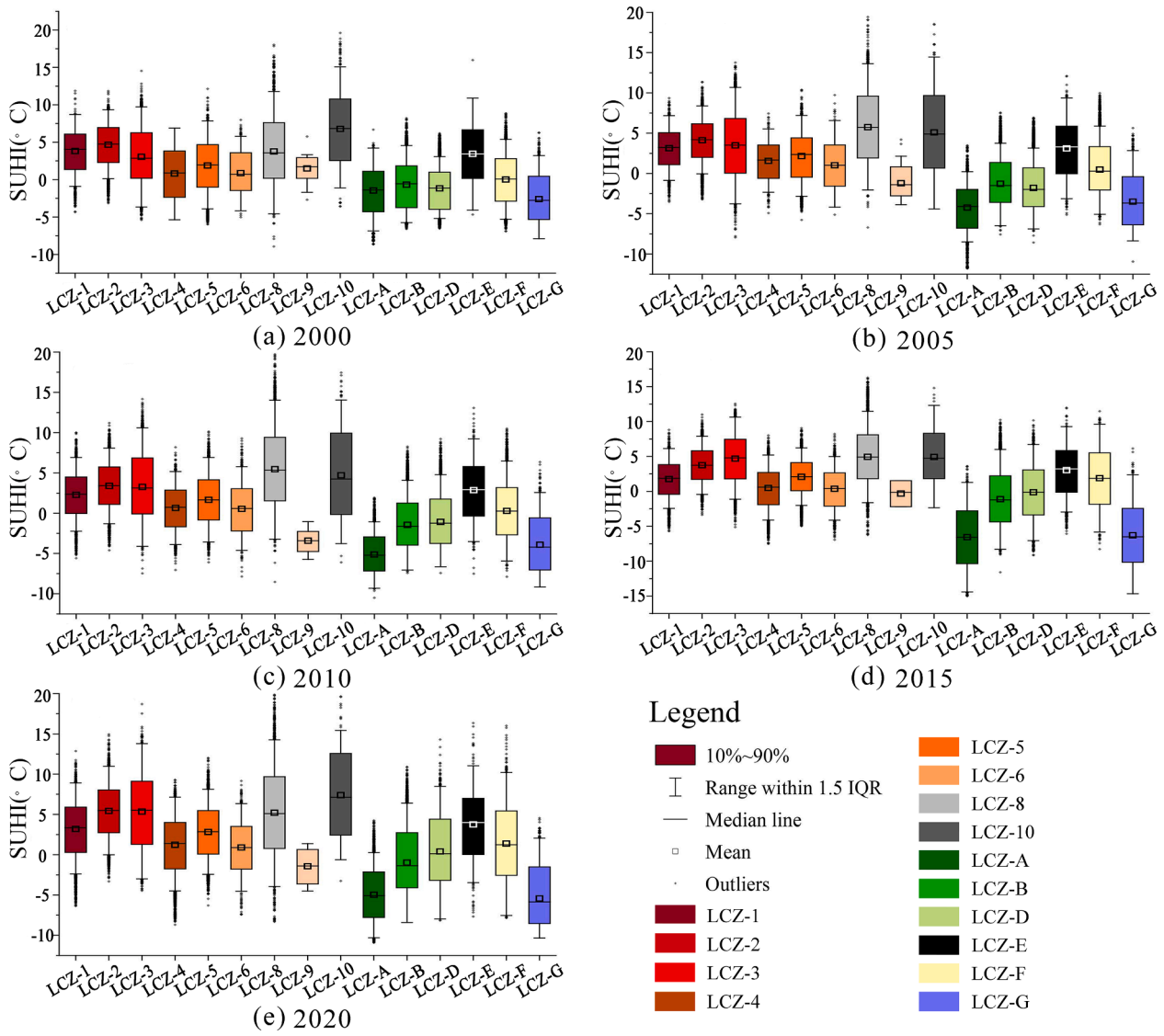


Fig. 9. Box plots of SUHI in different LCZ classes from 2000 to 2020.

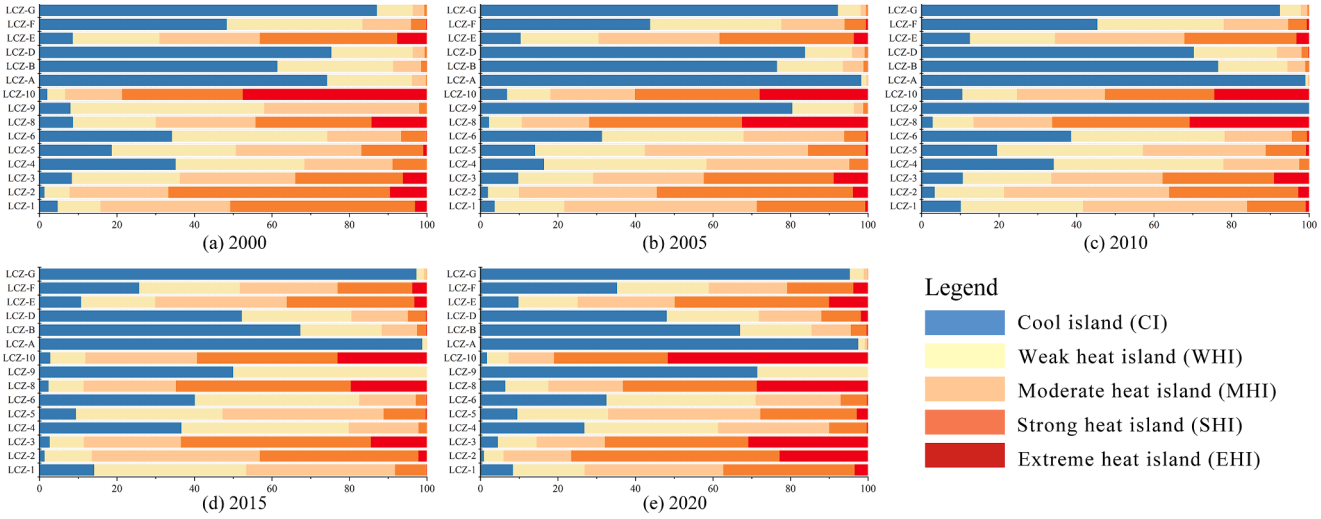


Fig. 10. SUHI composition in each LCZ classes in (a) 2000, (b) 2005, (c) 2010, (d) 2015, and (e) 2020.

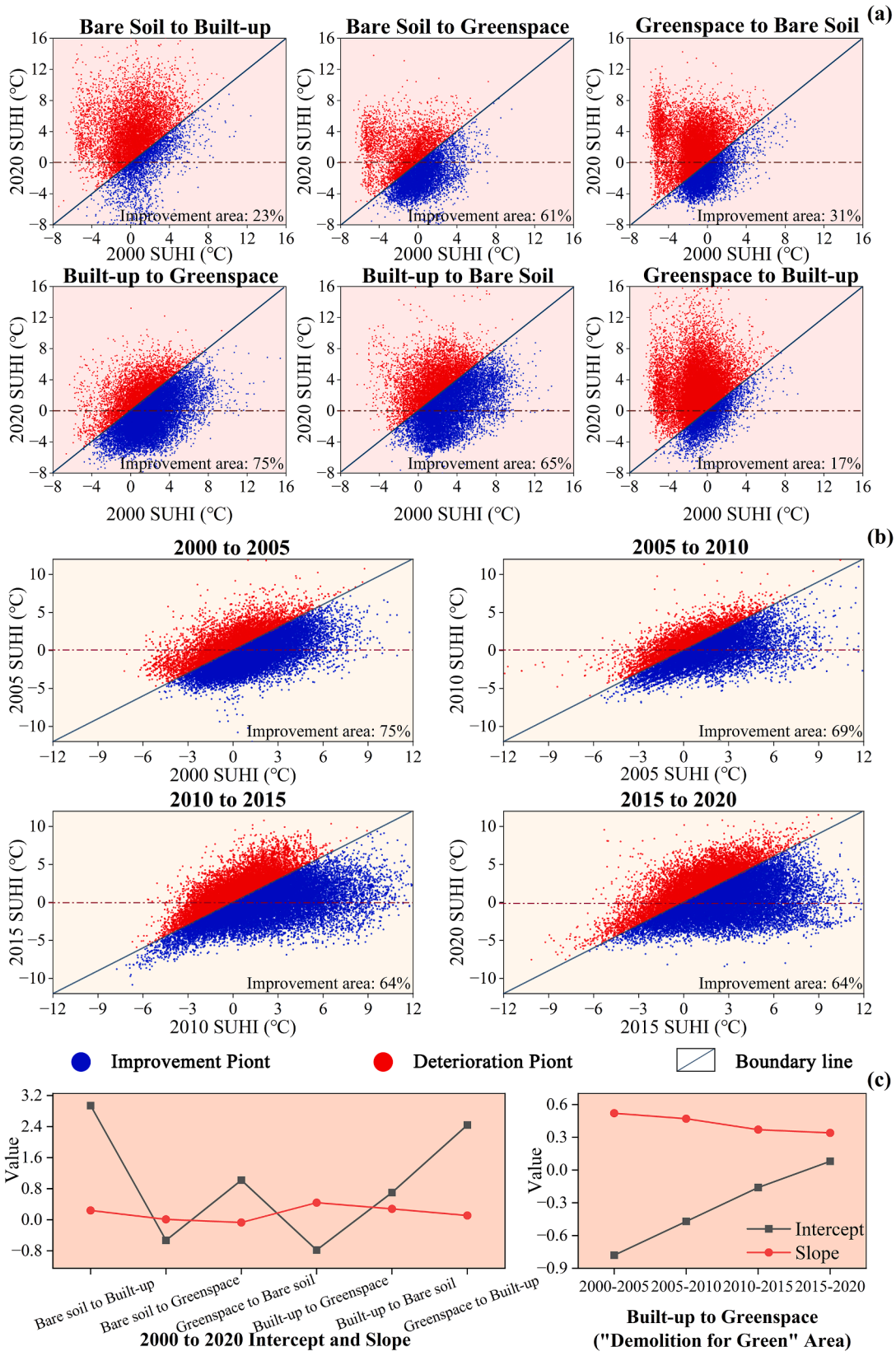


Fig. 11. (a) Fitting analysis results of SUHI for different land-use transitions from 2000 to 2020, (b) SUHI temporal fitting analysis for "Demolition for Green" areas every five years from 2000 to 2020, (c) Fitting results of intercept and slope. (Note: Above the blue line indicates worsening of the thermal environment, and below the blue line indicates improvement).

was on large-scale demolition of urban villages and the relocation of wholesale markets, targeting high-heat zones in central areas to maximize localized thermal improvements. From 2005 to 2015, while the cooling effect remained notable, it slightly diminished. The rise of high-rise buildings and increased construction density in suburban areas partially offset the thermal benefits of newly added green spaces. From 2015 to 2020, the cooling effect, though still significant, continued to diminish relative to earlier periods, largely due to accelerated urbanization and the compounded influence of climate change, which reduced the effectiveness of green space restoration in improving the thermal environment. Additionally, the focus of "Demolition for Green" shifted towards macro-scale ecological integration, prioritizing long-term resilience over immediate thermal gains, as demonstrated by projects like the Yongding River Ecological Restoration. This suggests that although the "Demolition for Green" measures overall have a positive effect in mitigating the urban heat island effect, the heat stress resulting from urban expansion remains a significant challenge.

Geographically weighted regression (GWR) model was used to further explore the relationship between the "Demolition for Green" policy and urban thermal environments, with SUHI change values as the dependent variable and the area ratio of "Demolition for Green" as the explanatory variable, the specific results are shown in Table 4. All models had R^2 values greater than 0.5, and the area ratio of "Demolition for Green" have a negative Coefficient with SUHI change values, which indicating that the regression analysis results are robust and effectively demonstrate the mitigating effect of the "Demolition for Green" policy on the urban thermal environment.

4. Discussions and limitations

4.1. Impact of LCZ changes on SUHI

Beijing's SUHI effect is largely shaped by urban morphology changes, leading to significant regional differences in the thermal environment distribution. Within Beijing's Sixth Ring Road, there is a clear trend of built-up classes having higher SUHI than natural land cover classes, with SUHI progressively increasing as building density rises. This aligns with findings from studies in other cities. For instance, a study in Shanghai showed that built environment factors significantly impact summer SUHI intensity. The average SUHI intensity in Shanghai's main urban area followed a spiraling trend from 2016 to 2020, increasing from 2.53 °C in 2016 to 3.04 °C in 2020, reflecting a worsening SUHI issue over these five years (Zeng et al., 2023). Similarly, research in Delhi indicates a positive correlation between the change in built-up areas and the rise in mean LST, which increased from 29.8 °C to 31.6 °C between 2007 and 2020. The rise in surface temperatures was also linked to an increase in UHI intensity (Ghosh et al., 2022). Despite the "Demolition for Green" policy promoting greening upgrades in some areas, the expansion of green spaces has not fully offset the thermal environment deterioration caused by the growth of built-up areas. From 2000 to 2020, 143 km^2 of built-up land was converted to green space, while 324 km^2 of green space was transformed into built-up areas. Particularly in the area between the Fourth and Sixth Ring Roads, although there has been some expansion of green spaces, the increase in building density, especially the growth of LCZ-1 and LCZ-8, has maintained a significant SUHI effect in this region. The "Demolition for Green" policy has also contributed to the transformation of LCZ-3 and LCZ-8 to some extent. Certain areas, originally consisting of LCZ-3, were converted into LCZ-B or LCZ-F due to demolition, resulting in a short-term increase in the cool island effect. However, this effect has been insufficient to offset the impact of increasing building density in the core urban areas.

Table 4
Geographically weighted regression (GWR) results for "Demolition for Green" and SUHI change (2000–2020).

Time Period	2000 to 2005	2005 to 2010	2010 to 2015	2015 to 2020	2000 to 2020
R^2	0.64	0.58	0.68	0.78	0.82
Residual sum of squares	56,383	44,408	62,680	58,971	170,697
Akaike's Information Criterion Corrected (AICc)	120,130	96,989	135,833	136,667	292,736
Average Coefficient	−4.42	−4.54	−3.8	−6.04	−12.56
Average Intercept	−0.16	−0.5	0.33	0.46	1.08

4.2. Impact of the "Demolition for Green" policy on LCZ changes

From 2000 to 2020, Beijing's urban morphology underwent significant changes, closely linked to the implementation of several governmental policies (Fig. 12). Urban morphology has gradually transitioned from compact to more open forms.

The implementation of the Beijing City Master Plan (2004–2020) facilitated the dispersal of functions from the central urban area through measures such as demolishing urban villages and relocating wholesale markets, which accelerated the expansion of built-up land in the peripheral regions. Low-rise (LCZ-3, LCZ-6) saw a significant reduction, while high-rise building land (LCZ-1, LCZ-4) showed an increasing trend. This indicates that while urban policies have promoted the dispersal of central functions, they also increase the intensity of construction.

The changes in green space were also significantly influenced by policy. From 2000 and 2010, green space declined due to the expansion of built-up areas. However, policies such as "Reduction Planning" and "Leave Space for Greenery" reversed this trend post-2010, slowing green space loss. The increase in scattered trees (LCZ-B) reflects qualitative improvements in green space development, consistent with the green development goals of the Beijing City Master Plan (2016–2035).

The analysis of LCZ transitions reveals that policy implementation has accelerated transformation between different LCZ classes. The shift from compact low-rise (LCZ-3) to large low-rise (LCZ-8) is particularly notable, which is directly related to the policy of expanding urban development to peripheral regions. Meanwhile, within the natural types, low plants (LCZ-D) have gradually transitioned into LCZ-B, particularly driven by the construction of green rings. 56 % of Beijing's "Demolition for Green" areas, covering an area of 79.85 km^2, are located within the two greenbelt zones, indicating that the policy has a significant impact on these areas. The areas outside the green rings were mostly influenced by specific demolition and greening plans, such as the "Comprehensive Governance and Ecological Restoration Green Construction Implementation Plan for the Yongding River in Beijing," which plans to relocate the Shougang Industrial Park and add 126 km^2 of forest parks. This process has significantly improved the ecological function of the urban periphery and established continuous ecological corridors, emphasizing the substantial impact of the "Demolition for Green" policy on these regions.

In addition, the World Health Organization recommends a minimum provision of 9 m^2 of urban green space per person, with an ideal value of up to 50 m^2. From 2000 to 2020, Beijing's park green spaces increased by 227.14 km^2. Given Beijing's current population of 21.89 million, this expansion corresponds to an average increase of 10.38 m^2 of urban green space per person—already exceeding the WHO minimum standard. When combined with the pre-existing green space, the overall per capita green area is likely to be even higher, indicating a significant improvement in addressing the ecological deficit. In fact, the newly added green space alone has achieved an ecological surplus equivalent to 30.13 km^2. This indicates that during urban development, policies have optimized the allocation of construction land, enhanced the connectivity of green spaces, and improved ecological benefits.

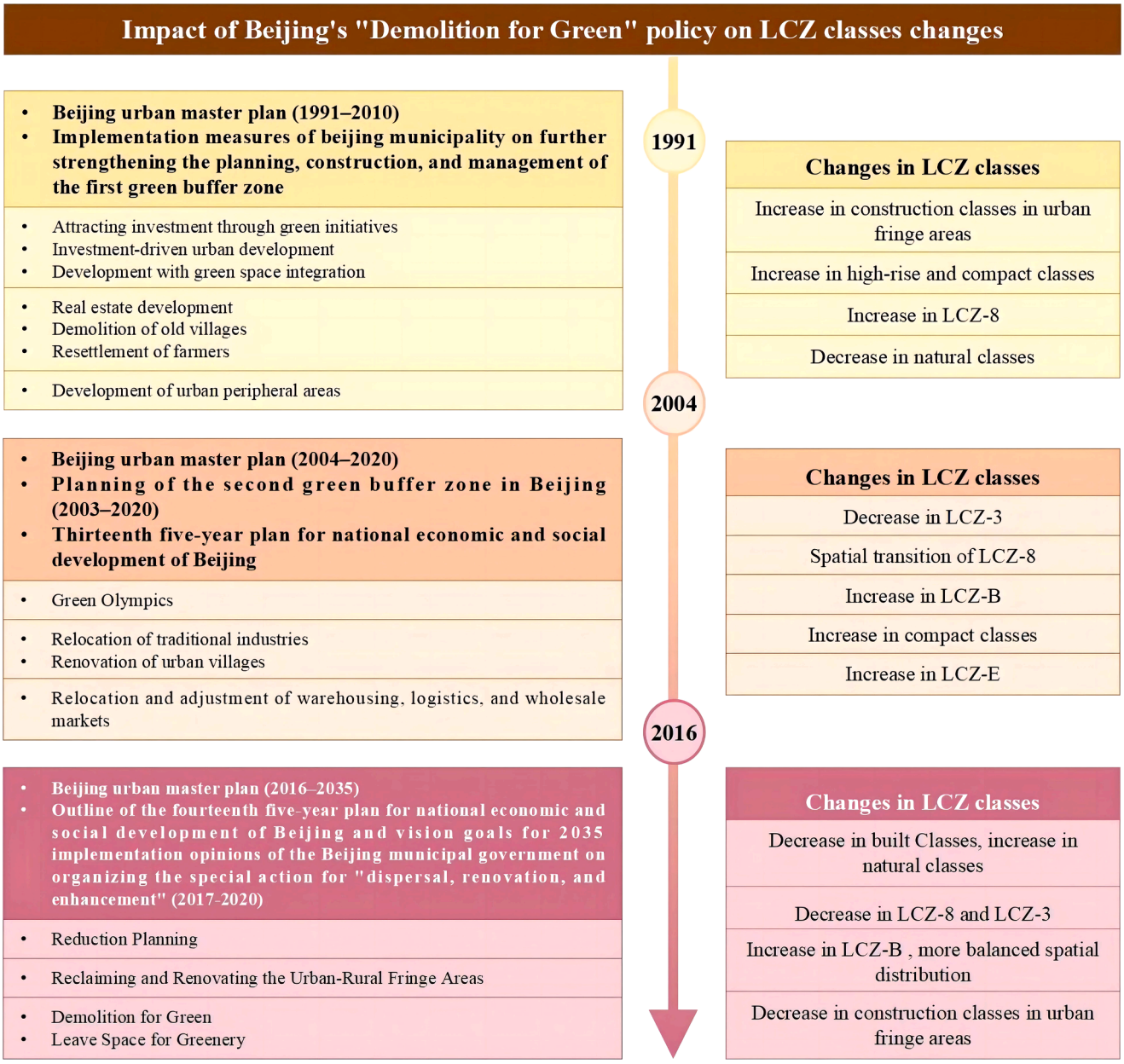


Fig. 12. Influence of Beijing's planning policies on LCZ transitions.

4.3. Impact of the "Demolition for Green" policy on urban thermal environment

Research on urban tree protection policies in Texas, USA, showed that areas impacted by the policy had LSTs 1.5 °C to 3.9 °C lower than control areas (Sung, 2013). This demonstrates the potential of targeted green policies to mitigate urban heat island effects. A study in China on urban greening through ecological restoration found that greening measures significantly slowed urban warming. The cooling potential in the urban core was about 1.01 °C, contributing to 56.08 % of the reduction in urban warming, over seven times higher than in urban sprawl areas (Xu et al., 2024). This underscores the importance of large-scale ecological restoration and vegetation management. Research in Duisburg, Germany, showed that publicly reduced 58 % of direct and thermal radiation within their range (Scholz et al., 2018). These studies underline the importance of urban tree management and greening policies, further proving the potential effectiveness of greening policies in improving urban heat environments.

To visually illustrate the impact of the "Demolition for Green" policy on the urban thermal environment, areas converted from built-up classes to green spaces between 2000 and 2020 were identified, and SUHI in these areas was analyzed for both years (Fig. 13(a)). Additionally, four representative areas were selected and analyzed in detail using Google Earth imagery (Fig. 13(b)).

Area 1: Located in Haidian District, Beijing, this area is part of the important ecological restoration and landscape improvement project in the "Three Mountains and Five Gardens" region. Through the old village demolition and land clearance policy, green spaces were expanded to improve the living environment. The project began in 2009 and was completed around 2016. The original Beiwucun and low-end industrial buildings were demolished and transformed into Beiwucun Park and Liangshan Park. The impact of the "Demolition for Green" policy led to a significant increase in the cool island (CI) ratio, rising from 30 % in 2000 to 93 % by 2020. Area 2: Niuwangmiao Village, affected by Beijing's greenbelt urbanization policy, was transformed from a traditional urban village into public green space. The demolition started in 2007 and was

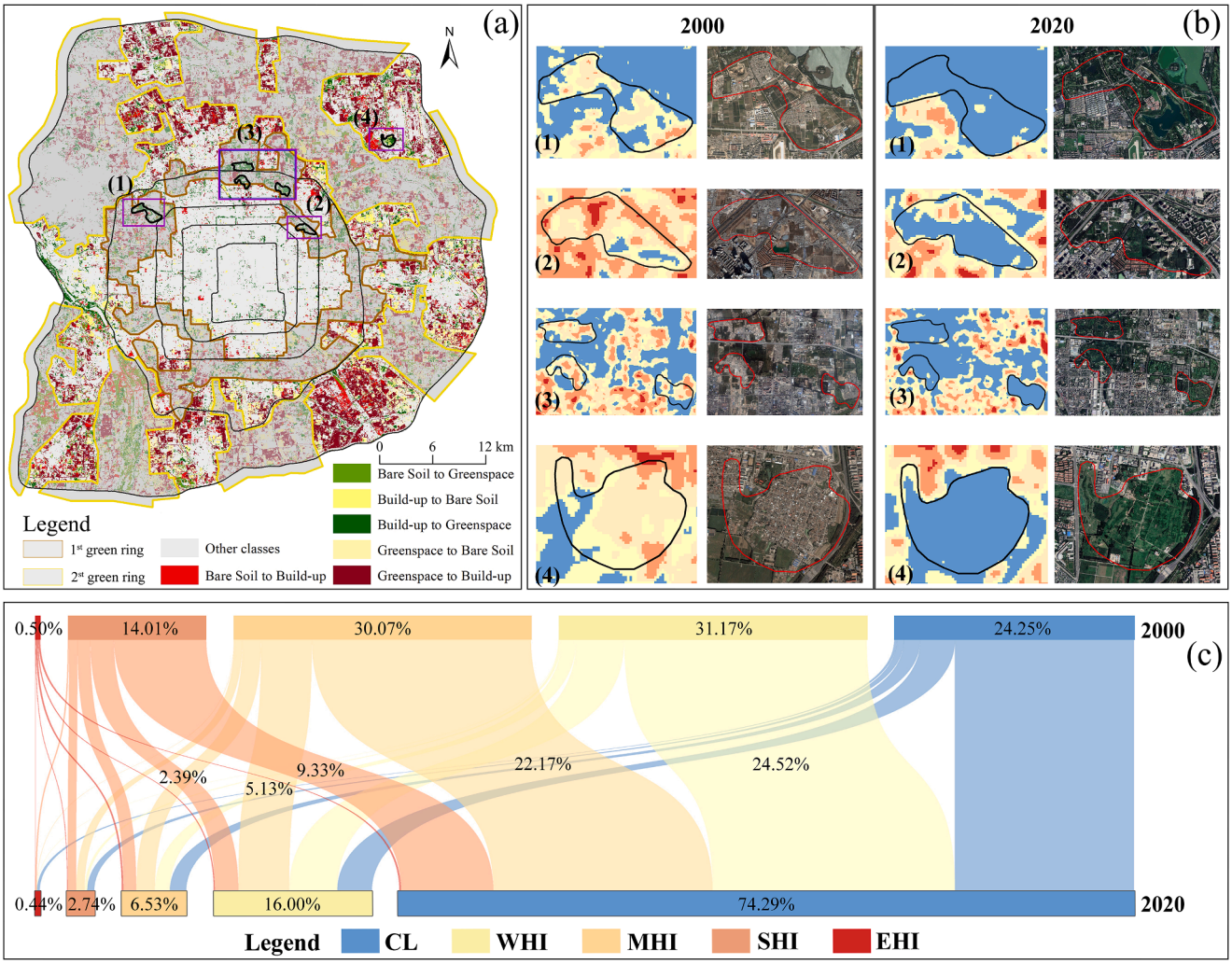


Fig. 13. (a) Land cover type transition map from 2000 to 2020; (b) Cooling effect slice map of the "Demolition for Green" areas; (c) SUHI variation map of the "Demolition for Green" Areas from 2000 to 2020.

completed by 2018. The cool island ratio in this area increased from 8 % in 2000 to 68 % by 2020. Area 3: The Beijing Olympic Forest Park, driven by the "Green Olympics" strategy, saw the demolition of low-efficiency buildings and old villages around the northern Fifth Ring Road in Chaoyang District, transforming the area into a large park. The design phase began in 2005, and the park was completed in 2008. The cool island ratio increased dramatically from 26 % in 2000 to 97 % in 2020. Area 4: Tianzhu Park, as part of the "decentralization and rectification for improvement" action, transformed inefficient land into green space, alleviating the urban heat island effect and improving residents' quality of life. The demolition began in 2009, and the park was completed in 2015. The cool island ratio rose from 9 % in 2000 to 96 % by 2020. Analysis of four case shows that the majority of UHI in these regions has been transformed into CI, indicating that the "Demolition for Green" policy effectively alleviates local thermal environments. Moreover, a reduction in UHI intensity was observed in the surrounding areas of policy implementation, with some SHI downgraded to WHI. This suggests that the policy not only improves thermal conditions in targeted regions but also exerts a spillover effect on adjacent areas.

By overlaying the spatial locations of "Demolition for Green" areas with SUHI data from 2000 to 2020, changes in SUHI within these areas over time were observed (Fig. 13(c)). The results indicate a notable increase in the CL area, while the areas of WHI, MHI, and SHI all decreased significantly. As a result, 56.02 % of these demolition areas transformed from heat islands to cool islands. However, the EHI area did not show a substantial reduction, and the total SUHI area remained around 25 %. This suggests that while the "Demolition for Green" policy effectively improves the thermal environment locally, it cannot fully offset the SUHI effects caused by high-intensity urban redevelopment.

Between 2000 and 2020, "Demolition for Green" areas were predominantly concentrated outside the Fourth Ring Road, aligning closely with the distribution of the two greenbelt zones. These areas experienced a significant reduction in SUHI, especially within the first greenbelt zone (inside the Fifth Ring Road), where demolition primarily involved LCZ-3. Following their transformation into LCZ-B, local thermal environments showed the most pronounced improvement. In contrast, the second greenbelt zone (between the Fifth and Sixth Ring Roads), which encompasses numerous rural-urban fringe villages, exhibited a relatively limited cooling effect due to its already low SUHI baseline.

Overall, while the "Demolition for Green" policy effectively alleviated local thermal stress, its scope and intensity were insufficient to counterbalance the overall SUHI increase driven by high-intensity urbanization and land development. Moreover, there was a spatial mismatch between new green spaces and newly developed urban areas. The green spaces were primarily added in the northern part of the city, while most new urban construction occurred in the southeast. This spatial discrepancy led to a reduction in high-temperature heat islands in the north but an increase in heat islands in the southeast.

4.4. Policy recommendations

Research shows that urban green spaces play a significant role in mitigating the UHI effect, particularly in areas with severe thermal conditions. Policymakers should prioritize increasing green spaces in these high-temperature regions to enhance the cooling effect of greenery. The "Demolition for Green" policy in the area between Beijing's Fourth and Fifth Ring Roads has shown the most significant effect, mainly due to the large and concentrated green space coverage in these areas. Although the thermal benefits of the "Demolition for Green" policy are evident, such demolition practices often lead to significant socioeconomic issues, including gentrification, demolition costs, disruption of social networks, and the displacement of vulnerable populations, as seen in cities like Addis Ababa and Accra, where informal workers and low-income residents are disproportionately affected (Weldegebriel et al., 2025). These disruptions are exacerbated by the displacement of social networks, which undermines community cohesion and economic stability (Sarpong et al., 2025). To address these challenges, urban planning must balance green space creation with the social costs of displacement. This can be achieved by integrating compensatory measures, such as alternative housing and financial support, and ensuring that affected communities are included in decision-making processes. Additionally, the spatial mismatch between high-density development and the location of green spaces can exacerbate UHI effects. The study found that while high-density development in the southeast of cities worsens UHI, green spaces in the north do not align with urban growth. Drawing lessons from historical urban renewal projects, such as the highway demolitions in São Paulo and Madrid, it is crucial to incorporate ecological structures like wind corridors and blue-green networks to prevent maladaptive outcomes. By doing so, cities can achieve a balance between development and cooling needs, avoiding further environmental and social issues (Stehlin & Millington, 2024).

Optimizing urban spatial morphology is key to alleviating the UHI effect. On a macro scale, planners should avoid the contiguous distribution of high-heat forms, such as heavy industry and large-scale low-rise buildings, and encourage the relocation of heat-intensive industries. On a micro scale, transforming existing built environments through vertical greening, permeable pavements, and renewable energy applications can reduce the need for large-scale demolition. Gradual updates should be prioritized to protect historical districts, thereby reducing potential social and cultural costs associated with sudden displacement.

4.5. Limitations and future studies

The study still has certain limitations. First, the limited spatial resolution of Landsat remote sensing imagery affects both heat island and green space detection. On the one hand, the relatively coarse resolution reduces the precision in identifying heat island boundaries, and on the other hand, it also limits the ability to detect small and fragmented green patches. This can lead to an underestimation of the mitigating effects of green spaces on urban heat island expansion. As a result, the conclusions about the effectiveness of green space interventions may be somewhat conservative. Future studies should incorporate higher-resolution thermal data or complementary datasets to better capture fine-scale thermal variations. Additionally, this research focuses on data from 2000 to 2020; expanding the time frame in future studies could provide reveal longer-term trends. Furthermore, while this study investigates the impact of the "Demolition for Green" policy on Beijing's urban thermal environment, it does not quantify specific demolition numbers or spatial distribution, instead offering a more macro-level analysis. This lack of specific data on the scale and location of demolitions means that the analysis cannot capture the full scope of the policy's spatial and temporal effects. Currently, the area converted to green space post-demolition is relatively small. Future studies could use simulation software to predict changes in heat island patterns resulting from large-scale demolitions and conversions to green spaces, providing valuable guidance for future urban planning in Beijing and other cities. Another limitation of this study is related to the use of LCZ for identifying three-dimensional urban morphology, with an overall accuracy of approximately 0.65. While this accuracy is sufficient for mesoscale studies, uncertainties remain, and improvements are needed. Specifically, when identifying green spaces, LCZ-B and LCZ-D share similar characteristics, and although five parameters were used to differentiate them, some regions still experience misclassification. In future studies, it is important to consider additional three-dimensional parameters and expand the number of categories to improve the accuracy of classification.

In summary, this study provides valuable references for future urban planning, particularly in balancing ecological restoration with high-density urban development. The limitations identified in this study, particularly related to spatial resolution and temporal scope, suggest that future research should aim to refine the analysis using more granular data and longer time frames. Future research could also explore the relationship between LCZ classes transition trends and other environmental variables (e.g., climate change, population growth), to offer policymakers more comprehensive decision-making support.

5. Conclusions

This study aims to examine whether the "Demolition for Green" policy is effective in mitigating the urban thermal environment. Therefore, this study analyzes the spatiotemporal variations of LCZ, LST, and SUHI within Beijing's Sixth Ring Road, revealing the complex relationship between urban morphology and the thermal environment. It also explores the role of the "Demolition for Green" policy in shaping urban morphology and regulating the thermal environment, providing valuable theoretical insights for urban planning and policy formulation.

(1) From 2000 and 2020, Beijing's built-up area expanded by 189.61 km^2, while green space decreased by 211.1 km^2. The LCZ structure shifted towards higher-intensity development, with low-rise forms continuously shrinking and a clear transition to high-rise forms. However, due to the implementation of the "Demolition for Green" policy, park green spaces increased by 227.14 km^2, and the area of "Demolition for Green" areas reached 143.38 km^2.
(2) Beijing's overall SUHI has shown an upward trend. Specifically, the heat island area within the Sixth Ring Road increased by 148.12 km^2, and the SUHI intensity rose from 0.98 °C in 2000 to 1.61 °C in 2020.
(3) Under the "Demolition for Green" policy, a large portion of compact low-rise (LCZ-3) and large low-rise (LCZ-8) within the Fourth Ring has been transformed into scattered trees (LCZ-B). Meanwhile, a significant amount of low plants (LCZ-D) beyond the Fourth Ring has shifted to LCZ-F, which in turn has been converted into LCZ-8. In terms of urban thermal environment, the "Demolition for Green" policy effectively improves the thermal environment in specific areas by influencing urban morphology, but it is challenging to offset the negative thermal impacts of high-intensity rapid urbanization.

Overall, in urban planning and management practices, implementing the "Demolition for Green" policy in areas with high UHI intensity and significant environmental stress can effectively improve the thermal environment. In dense urban areas where demolition is not feasible, measures such as rooftop greening and vertical greening can be adopted to increase greenery and enhance the ecological service functions of the area, thereby mitigating heat stress. Furthermore, the "Demolition for Green" policy can be utilized to create urban green corridors, leveraging ecological connectivity and scale effects to alleviate regional heat stress. During planning and implementation, it is essential to focus on balancing the spatial distribution of green spaces and built-up areas to avoid spatial mismatches, thereby maximizing the ecological benefits

and heat mitigation effects of green spaces.

CRediT authorship contribution statement

Linchun Zhang: Writing – original draft, Resources, Formal analysis, Data curation, Conceptualization. **Zhi Cai:** Writing – review & editing, Funding acquisition, Formal analysis, Data curation, Conceptualization. **Huanchun Huang:** Project administration, Methodology, Data curation, Conceptualization. **Zefeng Lu:** Writing – review & editing, Visualization, Validation, Supervision. **Wei Zhai:** Supervision, Software, Resources, Project administration. **Haoming Qin:** Visualization, Validation, Supervision, Software. **Zhifeng Liu:** Writing – review & editing, Validation, Supervision, Software, Resources. **Yan Tang:** Writing – review & editing, Software, Resources, Project administration, Methodology.

Declaration of competing interest

The authors declare that they have no known competing financial interests or personal relationships that could have appeared to influence the work reported in this paper.

Acknowledgments

This study was supported by Social Science Foundation of LinPing (Lpsk24C06).

Supplementary materials

Supplementary material associated with this article can be found, in the online version, at doi:10.1016/j.scs.2025.106576.

Data availability

Data will be made available on request.

References

Amati, M., & Yokohari, M. (2006). Temporal changes and local variations in the functions of London's green belt. *Landscape and Urban Planning, 75*(1), 125–142. https://doi.org/10.1016/j.landurbplan.2004.12.007

Arsad, F. S., Hod, R., Ahmad, N., Ismail, R., Mohamed, N., Baharom, M., Osman, Y., Radi, M. F. M., & Tangang, F. (2022). The impact of heatwaves on mortality and morbidity and the associated vulnerability factors: A systematic review. *International Journal of Environmental Research and Public Health, 19*(23), Article 16356. https://doi.org/10.3390/ijerph192316356

Ballester, J., Quijal-Zamorano, M., Mendez Turrubiates, R. F., Pegenaute, F., Herrmann, F. R., Robine, J. M., Basagana, X., Tonne, C., Anto, J. M., & Achebak, H. (2023). Heat-related mortality in Europe during the summer of 2022. *Nature Medicine, 29*(7), 1857–1866. https://doi.org/10.1038/s41591-023-02419-z

Bechtel, B., Alexander, P. J., Beck, C., Böhner, J., Brousse, O., Ching, J., Demuzere, M., Fonte, C., Gál, T., Hidalgo, J., Hoffmann, P., Middel, A., Mills, G., Ren, C., See, L., Sismanidis, P., Verdonck, M. L., Xu, G., & Xu, Y. (2019). Generating WUDAPT level 0 data - current status of production and evaluation. *Urban Climate, 27*, 24–45. https://doi.org/10.1016/j.uclim.2018.10.001

Beijing Municipal Bureau of Statistics. Beijing Statistical Yearbook. https://nj.tjj.beijing.gov.cn/nj/main/2021-tjnj/zk/indexch.htm, 2021 (accessed 23 November 2024).

Besir, A. B., & Cuce, E. (2018). Green roofs and facades: A comprehensive review. *Renewable and Sustainable Energy Reviews, 82*, 915–939. https://doi.org/10.1016/j.rser.2017.09.106

Cai, Z., Demuzere, M., Tang, Y., & Wan, Y. (2022). The characteristic and transformation of 3D urban morphology in three Chinese mega-cities. *Cities (London, England), 131*. https://doi.org/10.1016/j.cities.2022.103988

Chen, B., Xie, M., Feng, Q., Wu, R., & Jiang, L. (2022). Diurnal heat exposure risk mapping and related governance zoning: A case study of Beijing, China. *Sustainable Cities and Society, 81*, Article 103831. https://doi.org/10.1016/j.scs.2022.103831

Chen, L., Qi, Q., Wu, H., Feng, D., & Zhu, E. (2023). Will the landscape composition and socio-economic development of coastal cities have an impact on the marine cooling effect? *Sustainable Cities and Society, 89*, Article 104328. https://doi.org/10.1016/j.scs.2022.104328

Chinese Government. Beijing demolished nearly 60 million square meters of illegal construction in 2017, reclaiming land for greening. https://www.gov.cn/xinwen/2018-01/24/content_5260204.htm, 2018.

Chu, E., Anguelovski, I., & Roberts, D. (2017). Climate adaptation as strategic urbanism: Assessing opportunities and uncertainties for equity and inclusive development in cities. *Cities (London, England), 60*, 378–387. https://doi.org/10.1016/j.cities.2016.10.016

Deilami, K., Kamruzzaman, M., & Liu, Y. (2018). Urban heat island effect: A systematic review of spatio-temporal factors, data, methods, and mitigation measures. *International Journal of Applied Earth Observation and Geoinformation, 67*, 30–42. https://doi.org/10.1016/j.jag.2017.12.009

Demuzere, M., Kittner, J., & Bechtel, B. (2021). LCZ Generator: A web application to create local climate zone maps. *Frontiers In Environmental Science, 9*. https://doi.org/10.3389/fenvs.2021.637455

Du, H., Wang, D., Wang, Y., Zhao, X., Qin, F., Jiang, H., & Cai, Y. (2016). Influences of land cover types, meteorological conditions, anthropogenic heat and urban area on surface urban heat island in the Yangtze River Delta Urban Agglomeration. *Science of The Total Environment, 571*, 461–470. https://doi.org/10.1016/j.scitotenv.2016.07.012

Dutta, K., Basu, D., & Agrawal, S. (2021). Synergetic interaction between spatial land cover dynamics and expanding urban heat islands. *Environmental Monitoring and Assessment, 193*(4), 184. https://doi.org/10.1007/s10661-021-08969-4

Ebi, K. L., Capon, A., Berry, P., Broderick, C., de Dear, R., Havenith, G., Honda, Y., Kovats, R. S., Ma, W., Malik, A., Morris, N. B., Nybo, L., Seneviratne, S. I., Vanos, J., & Jay, O. (2021). Hot weather and heat extremes: Health risks. *The Lancet, 398*(10301), 698–708. https://doi.org/10.1016/S0140-6736(21)01208-3

Ghosh, S., Kumar, D., & Kumari, R. (2022). Assessing spatiotemporal variations in land surface temperature and SUHI intensity with a cloud based computational system over five major cities of India. *Sustainable Cities and Society, 85*, Article 104060. https://doi.org/10.1016/j.scs.2022.104060

Geletič, J., Lehnert, M., Savić, S., & Milošević, D. (2019). Inter-/intra-zonal seasonal variability of the surface urban heat island based on local climate zones in three central European cities. *Building and Environment, 156*, 21–32. https://doi.org/10.1016/j.buildenv.2019.04.011

Guo, J., Han, G., Xie, Y., Cai, Z., & Zhao, Y. (2020). Exploring the relationships between urban spatial form factors and land surface temperature in mountainous area: A case study in Chongqing city, China. *Sustainable Cities and Society, 61*, Article 102286. https://doi.org/10.1016/j.scs.2020.102286

Han, S., Hou, H., Estoque, R. C., Zheng, Y., Shen, C., Murayama, Y., Pan, J., Wang, B., & Hu, T. (2023). Seasonal effects of urban morphology on land surface temperature in a three-dimensional perspective: A case study in Hangzhou, China. *Building and Environment, 228*, Article 109913. https://doi.org/10.1016/j.buildenv.2022.109913

Hu, D., Meng, Q., Zhang, L., & Zhang, Y. (2020). Spatial quantitative analysis of the potential driving factors of land surface temperature in different "Centers" of polycentric cities: A case study in Tianjin, China. *Science of The Total Environment, 706*, Article 135244. https://doi.org/10.1016/j.scitotenv.2019.135244

Huang, X., & Wang, Y. (2019). Investigating the effects of 3D urban morphology on the surface urban heat island effect in urban functional zones by using high-resolution remote sensing data: A case study of Wuhan, Central China. *ISPRS Journal of Photogrammetry and Remote Sensing, 152*, 119–131. https://doi.org/10.1016/j.isprsjprs.2019.04.010

Iungman, T., Cirach, M., Marando, F., Pereira Barboza, E., Khomenko, S., Masselot, P., Quijal-Zamorano, M., Mueller, N., Gasparrini, A., Urquiza, J., Heris, M., Thondoo, M., & Nieuwenhuijsen, M. (2023). Cooling cities through urban green infrastructure: A health impact assessment of European cities. *The Lancet, 401*(10376), 577–589. https://doi.org/10.1016/S0140-6736(22)02585-5

Jabbar, H. K., Hamoodi, M. N., & Al-Hameedawi, A. N. (2023). Urban heat islands: A review of contributing factors, effects and data. In *, 1129. IOP conference series: Earth and environmental science*, Article 012038. https://doi.org/10.1088/1755-1315/1129/1/012038

Johnson, S., Ross, Z., Kheirbek, I., & Ito, K. (2020). Characterization of intra-urban spatial variation in observed summer ambient temperature from the New York city community air survey. *Urban Climate, 31*, Article 100583. https://doi.org/10.1016/j.uclim.2020.100583

Lemoine-Rodríguez, R., Inostroza, L., Falfán, I., & MacGregor-Fors, I. (2022). Too hot to handle? On the cooling capacity of urban green spaces in a Neotropical Mexican city. *Urban Forestry & Urban Greening, 74*, Article 127633. https://doi.org/10.1016/j.ufug.2022.127633

Li, Z. L., Wu, H., Duan, S. B., Zhao, W., Ren, H., Liu, X., Leng, P., Tang, R., Ye, X., Zhu, J., Sun, Y., Si, M., Liu, M., Li, J., Zhang, X., Shang, G., Tang, B. H., Yan, G., & Zhou, C. (2023). Satellite remote sensing of global land surface temperature: Definition, methods, products, and applications. *Reviews of Geophysics, 61*(1). https://doi.org/10.1029/2022rg000777

Liang, H., Meng, Q., Qi, Q., & Ren, P. (2022). Spatiotemporal interaction between urban heat island and urban-construction indicators on the block scale in autumn in a humid and hot climate. *Sustainable Cities and Society, 78*, Article 103638. https://doi.org/10.1016/j.scs.2021.103638

Liao, W., Guldmann, J.-M., Hu, L., Cao, Q., Gan, D., & Li, X. (2023). Linking urban park cool island effects to the landscape patterns inside and outside the park: A simultaneous equation modeling approach. *Landscape and Urban Planning, 232*, Article 104681. https://doi.org/10.1016/j.landurbplan.2022.104681

Liao, W., Hong, T., & Heo, Y. (2021). The effect of spatial heterogeneity in urban morphology on surface urban heat islands. *Energy and Buildings, 244*, Article 111027. https://doi.org/10.1016/j.enbuild.2021.111027

Liu, W., Zhang, L., Hu, X., Meng, Q., Qian, J., Gao, J., & Li, T. (2024). Nonlinear effects of urban multidimensional characteristics on daytime and nighttime land surface temperature in highly urbanized regions: A case study in Beijing, China. *International Journal of Applied Earth Observation and Geoinformation, 132*, Article 104067. https://doi.org/10.1016/j.jag.2024.104067

Liu, Y., Li, H., Gao, P., & Zhong, C. (2020). Monitoring the detailed dynamics of regional thermal environment in a developing urban agglomeration. *Sensors, 20*(4). https://doi.org/10.3390/s20041197

Liu, Z., Cheng, K. Y., Amati, M., Jim, C. Y., Hua, C., Yokohari, M., Cameron, R., & Ng, E. (2025). Creating a thermally comfortable city through urban green infrastructure: An international review of greening policies. *Urban Forestry & Urban Greening, 105*, Article 128713. https://doi.org/10.1016/j.ufug.2025.128713

Ma, Y., Mamitimin, Y., Tiemuerbieke, B., Yimaer, R., Huang, M., Chen, H., Tao, T., & Guo, X. (2023). Spatiotemporal characteristics and influencing factors of urban heat island based on geographically weighted regression model: A case study of Urumqi City. *Land, 12*(11). https://doi.org/10.3390/land12112012

Meng, F., Zhang, L., Ren, G., & Zhang, R. (2023). Impacts of UHI on variations in cooling loads in buildings during heatwaves: A case study of Beijing and Tianjin, China. *Energy, 273*, Article 127189. https://doi.org/10.1016/j.energy.2023.127189

Moazzam, M. F. U., Doh, Y. H., & Lee, B. G. (2022). Impact of urbanization on land surface temperature and surface urban heat Island using optical remote sensing data: A case study of Jeju Island, Republic of Korea. *Building and Environment, 222*, Article 109368. https://doi.org/10.1016/j.buildenv.2022.109368

Moazzam, M. F. U., & Lee, B. G. (2024). Urbanization influenced SUHI Of 41 megacities of the world using big geospatial data assisted with google earth engine. *Sustainable Cities and Society, 101*, Article 105095. https://doi.org/10.1016/j.scs.2023.105095

Oke, T. R., & Stewart, I. D. (2012). Local climate zones for urban temperature studies. *Bulletin of the American Meteorological Society, 93*(12), 1879–1900. https://doi.org/10.1175/bams-D-11-00019.1

Portela, C. I., Massi, K. G., Rodrigues, T., & Alcântara, E. (2020). Impact of urban and industrial features on land surface temperature: Evidences from satellite thermal indices. *Sustainable Cities and Society, 56*, Article 102100. https://doi.org/10.1016/j.scs.2020.102100

Qiang, H., & Hu, L. (2022). Population and capital flows in metropolitan Beijing, China: Empirical evidence from the past 30 years. *Cities (London, England), 120*, Article 103464. https://doi.org/10.1016/j.cities.2021.103464

Ren, T., Zhou, W., & Wang, J. (2021). Beyond intensity of urban heat island effect: A continental scale analysis on land surface temperature in major Chinese cities. *Science of the Total Environment, 791*, Article 148334. https://doi.org/10.1016/j.scitotenv.2021.148334

Rizvi, S. H., Fatima, H., Iqbal, M. J., & Alam, K. (2020). The effect of urbanization on the intensification of SUHIs: Analysis by LULC on Karachi. *Journal of Atmospheric and Solar-Terrestrial Physics, 207*, Article 105374. https://doi.org/10.1016/j.jastp.2020.105374

Sarpong, A. O., Müller-Mahn, D., & Osei, O. E. (2025). Decoding the logics behind the demolition and redevelopment of Agbogbloshie Scrapyard, Accra, Ghana. *Geoforum; Journal of Physical, Human, and Regional Geosciences, 159*, Article 104180. https://doi.org/10.1016/j.geoforum.2024.104180

Scholz, T., Hof, A., & Schmitt, T. (2018). Cooling effects and regulating ecosystem services provided by urban trees—novel analysis approaches using urban tree cadastre data. *Sustainability, 10*(3). https://doi.org/10.3390/su10030712

Shao, L., Liao, W., Li, P., Luo, M., Xiong, X., & Liu, X. (2023). Drivers of global surface urban heat islands: Surface property, climate background, and 2D/3D urban morphologies. *Building and Environment, 242*, Article 110581. https://doi.org/10.1016/j.buildenv.2023.110581

Sheng, Q., Ji, Y., Jia, C., Jiang, L., Li, C., Huang, Z., Ma, C., Zhang, X., Chen, H., Wang, T., Zhu, Y., & Zhu, Z. (2025). Differential effects of cooling and humidification in urban green spaces and thresholds of vegetation community structure parameters: A case study of the Yangtze River Delta region. *Cities (London, England), 159*, Article 105765. https://doi.org/10.1016/j.cities.2025.105765

Stehlin, J., & Millington, N. (2024). De-infrastructuring automobility: The politics of urban highway repurposing and removal in São Paulo and Madrid. *Geoforum; Journal of Physical, Human, and Regional Geosciences, 152*, Article 104015. https://doi.org/10.1016/j.geoforum.2024.104015

Sung, C. Y. (2013). Mitigating surface urban heat island by a tree protection policy: A case study of The Woodland, Texas, USA. *Urban Forestry & Urban Greening, 12*(4), 474–480. https://doi.org/10.1016/j.ufug.2013.05.009

Tang, L., Zhan, Q., Fan, Y., Liu, H., & Fan, Z. (2023). Exploring the impacts of greenspace spatial patterns on land surface temperature across different urban functional zones: A case study in Wuhan metropolitan area, China. *Ecological Indicators, 146*. https://doi.org/10.1016/j.ecolind.2022.109787

The People's Government of Beijing Municipality. Notice of the people's government of Beijing municipality on issuing the '14th five-year plan' for major infrastructure development in Beijing. https://www.beijing.gov.cn/zhengce/zhengcefagui/20220303/t20220303_2621094.html, 2022 (accessed 4 June , 2025).

Tu, Y., Chen, B., Yang, J., & Xu, B. (2023). Olympic effects on reshaping urban greenspace of host cities. *Landscape and Urban Planning, 230*, Article 104615. https://doi.org/10.1016/j.landurbplan.2022.104615

Unal Cilek, M., & Cilek, A. (2021). Analyses of land surface temperature (LST) variability among local climate zones (LCZs) comparing Landsat-8 and ENVI-met model data. *Sustainable Cities and Society, 69*. https://doi.org/10.1016/j.scs.2021.102877

Wang, R., Voogt, J., Ren, C., & Ng, E. (2022). Spatial-temporal variations of surface urban heat island: An application of local climate zone into large Chinese cities. *Building and Environment, 222*, Article 109378. https://doi.org/10.1016/j.buildenv.2022.109378

Wei, S., He, Z., Zhai, W., Zhao, C., & Li, Y. (2025). How does vegetation influence surface temperature across various road types and urban morphology types? *Building and Environment, 270*, Article 112511. https://doi.org/10.1016/j.buildenv.2024.112511

Weldegebriel, A. T., Lombardo, A., Tekalign, M., Van Rompaey, A., & Janusz, K. (2025). Understanding Addis Ababa's urban transition and slum clearance through gentrification theory. *Cities (London, England), 162*, Article 105952. https://doi.org/10.1016/j.cities.2025.105952

Wu, Y., Patuano, A., Mashhoodi, B., Lenzholzer, S., Acred, A., & Narvaez Zertuche, L. (2025). How small green spaces cool urban neighbourhoods: Optimising distribution, size and shape. *Landscape and Urban Planning, 253*, Article 105224. https://doi.org/10.1016/j.landurbplan.2024.105224

Xiang, Z., Qin, H., He, B.-J., Han, G., & Chen, M. (2022). Heat vulnerability caused by physical and social conditions in a mountainous megacity of Chongqing, China. *Sustainable Cities and Society, 80*, Article 103792. https://doi.org/10.1016/j.scs.2022.103792

Xu, D., Bai, T., Yang, L., Zhou, Y., Chen, B., Xu, H., Song, Y., Yuan, Y., Cui, Y., Meng, L., Xia, Z., Chen, M., Xu, Z., Zhao, P., Dong, G., Zhang, L., Zhao, J., Wu, W., Wang, W., Zhao, L., Cheng, J., & Ciais, P. (2024). Quantifying the cooling effect of urban greening driven by ecological restoration projects in China. *Environmental Science & Technology, 58*(47), 20990–21001. https://doi.org/10.1021/acs.est.4c10314

Yang, J., Zhan, Y., Xiao, X., Xia, J. C., Sun, W., & Li, X. (2020). Investigating the diversity of land surface temperature characteristics in different scale cities based on local climate zones. *Urban Climate, 34*. https://doi.org/10.1016/j.uclim.2020.100700

Yang, K., Tao, F., Wang, C.-L., Wang, Z.-L., Han, Q.-L., & Zhou, T. (2023). An optimization method for surface urban heat island footprint extraction based on anisotropy assumption. *Urban Climate, 49*, Article 101532. https://doi.org/10.1016/j.uclim.2023.101532

Yin, C., Yuan, M., Lu, Y., Huang, Y., & Liu, Y. (2018). Effects of urban form on the urban heat island effect based on spatial regression model. *Science of the Total Environment, 634*, 696–704. https://doi.org/10.1016/j.scitotenv.2018.03.350

Yin, H., & Zhao, X. (2024). Urban heat island analysis based on high resolution measurement data: A case study in Beijing. *Sustainable Cities and Society, 106*, Article 105389. https://doi.org/10.1016/j.scitotenv.2017.11.327

Zeng, P., Zong, C., Duan, Z., & Wei, X. (2023). Exploring the spatial interplay between built-up environments and surface urban heat island phenomena in the main urban area of Shanghai. *Energy and Buildings, 301*, Article 113739. https://doi.org/10.1016/j.enbuild.2023.113739

Zhao, C., Zhu, H., Zhang, S., Jin, Z., Zhang, Y., Wang, Y., Shi, Y., Jiang, J., Chen, X., & Liu, M. (2024). Long−term trends in surface thermal environment and its potential drivers along the urban development gradients in rapidly urbanizing regions of China. *Sustainable Cities and Society, 105*. https://doi.org/10.1016/j.scs.2024.105324

Zhao, L., Oppenheimer, M., Zhu, Q., Baldwin, J. W., Ebi, K. L., Bou-Zeid, E., Guan, K., & Liu, X. (2018). Interactions between urban heat islands and heat waves. *Environmental Research Letters, 13*(3). https://doi.org/10.1088/1748-9326/aa9f73

Zhang, L., Wang, S., Zhai, W., He, Z., Shi, W., Li, Y., & Zhao, C. (2025). How does blue-green Infrastructure affect the urban thermal environment across various functional zones? *Urban Forestry & Urban Greening, 105*, Article 128698. https://doi.org/10.1016/j.ufug.2025.128698

Zhou, L., Gong, Y., López-Carr, D., & Huang, C. (2024). A critical role of the capital green belt in constraining urban sprawl and its fragmentation measurement. *Land Use Policy, 141*, Article 107148. https://doi.org/10.1016/j.landusepol.2024.107148